Geomorphology 472 (2025) 109587

Contents lists available at ScienceDirect

Geomorphology

journal homepage: www.journals.elsevier.com/geomorphology

Decoding Late Quaternary faulting through marine terraces and MIS 5.5 tilted tidal notches: Insights from central Mediterranean Sea (NW Sicily, Italy)

Mauro Agate [a], Fabrizio Antonioli [b], Francesco Caldareri [a], Stefano Devoto [c], Maurizio Gasparo Morticelli [a], Attilio Sulli [a], Nicolò Parrino [a,*], Stefano Furlani [c]

[a] Department of Earth and Marine Sciences, University of Palermo, 90123 Palermo, Italy
[b] CNR IGAG, Piazzale Aldo Moro 7, 00185 Rome, Italy
[c] Department of Mathematics, Informatics and Geosciences, University of Trieste, via Weiss 2, 34127 Trieste, Italy

ARTICLE INFO

Keywords:
Coastal Landscape Evolution
Tectonic Geomorphology
Southern Tyrrhenian Tectonic
Geoswim programme
Central Mediterranean Sea

ABSTRACT

This study investigates the recent tectonic evolution of coastal landscapes, focusing on integrating fossil tidal notches and fossil marine terraces as tools for coastal tectonic studies in the Capo Rama promontory (central Mediterranean, southern Italy, NW Sicily). These geomorphological features are crucial for understanding the tectonic forcings that shape coastal landscapes (e.g. active faulting or regional uplift), especially in the context of the high resolution topographic and morphometric data available today. This research addresses a significant gap in the current understanding of the combined use of these markers to study the evolution of the coastal landscape and its tectonic drivers. The aim is to elucidate the interplay between coastal geomorphology and tectonics in areas with elusive tectonic activity (i.e., regions deforming at a rate lesser than 1 mm/yr), hosting previously undetected seismogenic sources and, for that reason, assumed as having low seismic hazard. Employing a multidisciplinary approach, the study integrates surveys conducted along the emerged and submerged coastline with analytic/statistical morphometric analyses and fault modelling. This methodology offers a comprehensive view of the elevation and distribution of MIS 5.5 littoral deposits and coastal geomorphological markers such as marine terrace inner edges and tidal notches. Key findings reveal substantial elevation differences in these markers, varying between +34 and +1.9 m above sea level along a north-south transect, highlighting an active seaward tilting in the study area. Such tilting is related to the Quaternary deformation of a previously unknown buried fault crossing the study area. Achieved outcomes allowed exploring the integration of tidal notches and marine terraces' inner edges as geomorphological markers for coastal tectonic analyses. Moreover, this study lays foundations for future research, enabling a more detailed understanding of the hypothesized buried fault, and its contributions to the understanding of the active faulting processes in the southern Tyrrhenian region.

1. Introduction

Understanding the evolution of coastal landscapes by accurately tracing the historical and paleo-shoreline positions and their relative geomorphological markers is one of the most effective approaches for studying coastal tectonics (Parrino et al., 2023; Srivastava et al., 2023; Caldareri et al., 2024; Maltese et al., 2024; Malik et al., 2024). This approach often relies on specific geomorphological markers whose interpretation reveals the interplay between erosional processes, sediment deposition, and tectonic activities. Among these markers, Fossil Marine Terrace (FMT) have been predominantly utilized as paleo-geodetic markers for computing vertical differential movements and eustatic sea-level changes (Ferranti et al., 2009; Santoro et al., 2013; Komori et al., 2020; Racano et al., 2020; Robertson et al., 2020; Meschis et al., 2024). Rocky coasts tend to have erosional features as abrasion platforms representing the marine terraces covering over half of the Mediterranean basin (Furlani et al., 2014a). Part are plunging cliffs with a deep base below the water level (Sunamura, 1992). Such cliffs can easily preserve geomorphological markers of past sea levels, such as tidal notches. These notches are indentations or undercutting, ranging

* Corresponding author.
E-mail address: nicolo.parrino@unipa.it (N. Parrino).

https://doi.org/10.1016/j.geomorph.2024.109587
Received 15 January 2024; Received in revised form 26 December 2024; Accepted 28 December 2024
Available online 31 December 2024

from a few centimetres to several meters deep, formed in steep cliffs at or near sea level (Antonioli et al., 2015, 2018; Furlani et al., 2021). The tidal notches' elevation and morphotype can be successfully surveyed and sampled through coastal surveys to collect detailed and continuous data along broad sectors of the coastline (Furlani et al., 2017; Furlani, 2020; Furlani and Antonioli, 2023).

Whether FMT or Fossil Tidal Notch (FTN), the age estimation of sea-level indicators is a pivotal component of Quaternary coastal tectonic studies. Indeed, an accurate chronological assessment enables quantifying the rates of regional and local vertical differential movement over time. Such age-specific information is critical for developing reliable age models capable of enhancing the accuracy and interpretive power of coastal landscape evolution (Roberts et al., 2013; Lo Presti et al., 2014; Jara-Muñoz et al., 2019; De Gelder et al., 2020; Ferranti et al., 2021; Komori et al., 2021; Malatesta et al., 2022; Parrino et al., 2022; Pirrotta et al., 2022).

The age estimation of FTN offers a distinct approach for chronological analysis and rate calculations compared to FMT. Due to their rapid formation, tidal notches (TN) effectively record minor sea-level fluctuations with an accuracy ranging from few decimetres to centimetres in some cases observed along the coasts of the Mediterranean Sea (e.g. Antonioli et al., 2015). However, the relatively fixed morphology of TN limits their utility in recording extended periods of sea-level stability, even if useful to identify co-seismic displacements during sea-level stability periods (Pirazzoli and Evelpidou, 2013). Conversely, FMT is more practical at recording longer sea-level stability because these extended periods until 10.5 ka, such as the Marine Isotope Stage (MIS) 5.5 highstand, frequently result in wider terraced surfaces (Malatesta et al., 2022). Such dissimilar sensitivities of FTN and FMT to sea-level variations underscore their complementary roles in coastal tectonic studies.

Despite the apparent complementarity between TN and MT inner edges as geomorphic markers, existing research has poorly explored their synergistic application. This paper addresses this gap by evaluating the strengths and limitations of the combined use of FTN and inner edge and presenting newly collected data in NW Sicily. The Northern Sicilian Continental Margin (NSCM, Fig. 1) sector is an excellent study area due to its diverse coastal morphology, encompassing plunging cliffs and FMT. While previously considered geologically stable, recent studies that redefine the seismotectonic framework of the region highlighted the need for a more detailed investigation into Quaternary fault activity in it (Caracausi and Sulli, 2019; Sulli et al., 2021a, 2021b; Parrino et al., 2022).

This study employed a multidisciplinary approach, comprising surveys focused on the submerged coastline along an 8.57 km route of the Cape Rama cliff, field surveys, and the mapping of the marine terraces inner edge. The spatial distribution of the thus collected markers was used to invert the parameters of the fault that can be responsible for their

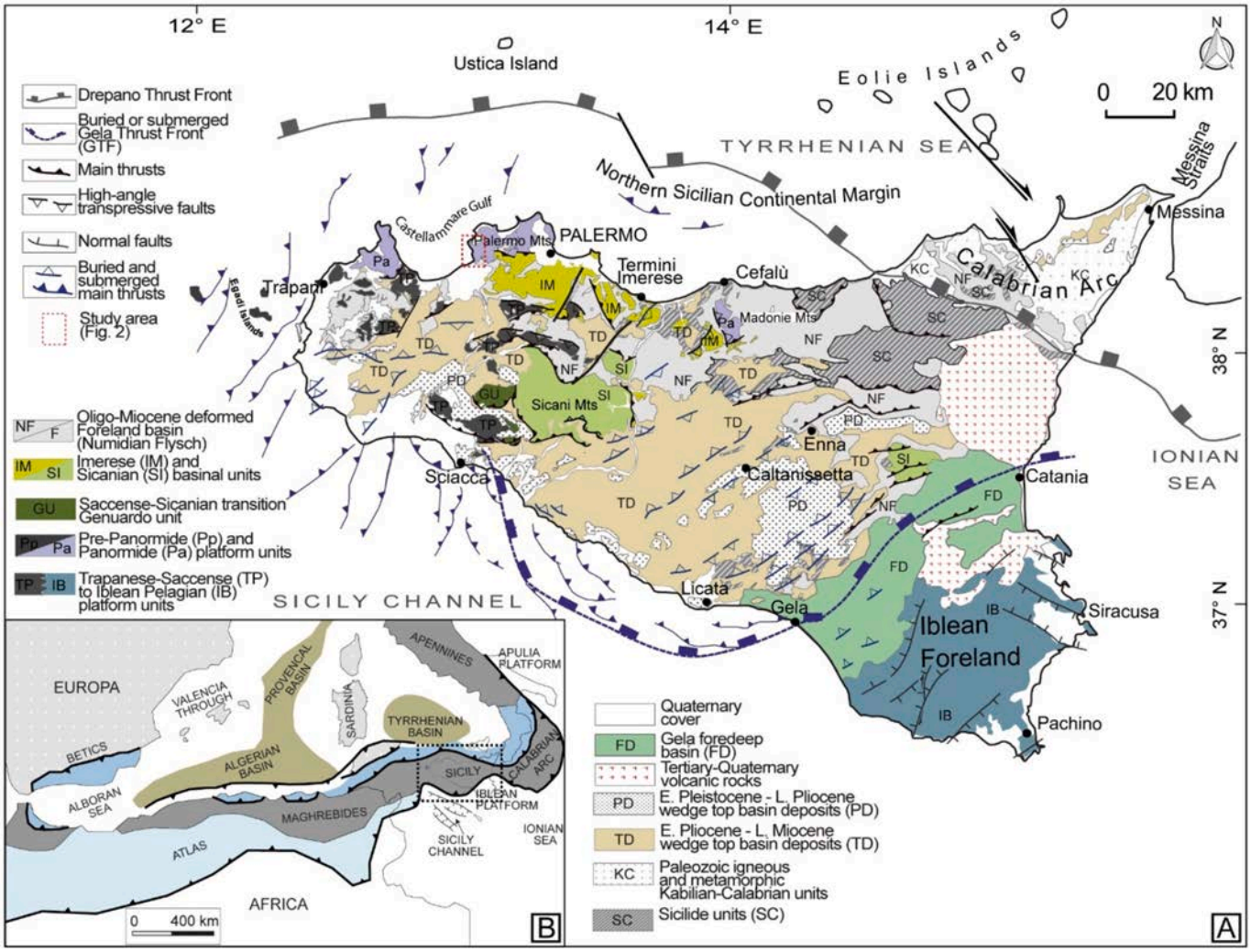

Fig. 1. A) The inset A displays a simplified geological map of Sicily, highlighting its most prominent lithologic domains and the tectonic units that characterize the Sicilian Fold and Thrust Belt. This representation has been modified from Catalano et al., 2013a. B) The inset B shows the regional geodynamic framework of the Central Mediterranean Sea, illustrating its main tectonic discontinuities.

deformation using a best-fit Okada approach (Okada, 1985). The results garnered from this inversion are utilized to infer a late Quaternary blind fault activity and to contextualize this activity within the broader seismotectonic framework of the study area.

1.1. The last Interglacial Highstand

The Marine Isotope Stage (MIS) 5 coincides with the last interglacial, and its timing is based on orbital tuning of high-resolution deep-sea oxygen isotope stratigraphy. According to this stratigraphy, the MIS 5.5 subunit occurred between Termination II (the end of MIS 6) and the onset of MIS 5.4. Regarding the dating of this highstand period, a vast body of literature has addressed it, beginning with the pioneering works of Emiliani (1955) and Shackleton and Opdyke (1973), who dated MIS 5.5 to span between 140 and 116 ka. More recent literature, based on coral dating and accounting for glacial and hydro-isostatic adjustment (GIA), has proposed narrowing this period to between 132 and 116 ka (Stirling et al., 1998; Bard et al., 2002; Shackleton et al., 2003; Kopp et al., 2009; Murray-Wallace and Woodroffe, 2014; Antonioli et al., 2018, 2020).

Sea level indicators formed during MIS 5.5 have been reported from over one thousand sites worldwide (Pedoja et al., 2011; Rovere et al., 2023). The elevation above the present sea level of the MIS 5.5 highstand, measured in globally stable areas, has previously been estimated based on coral reefs using various methods (Bard et al., 1990; Chen et al., 1991; Chappell et al., 1996; Schellmann and Radtke, 2004; Blanchon et al., 2009). These estimates show an uncertainty of some meters in assessing the paleo sea level (Muhs and Simmons, 2017) because corals do not accurately mark the sea level but the photic zone. Furthermore, in many regions of the world, coral reefs are absent and cannot be relied on to constrain the height of MIS 5.5 sea levels. Other geomorphological markers, such as speleothems or lagoonal fossil sediments, show a high altimetric precision (Ferranti et al., 2006; Antonioli et al., 2020;) but the present elevation of these makers can significantly change due to forcers such as glacio-hydro-isostasy, that play an important role at Quaternary timescales. Ice-driven sea-level changes stem from the contribution of ocean mass variation in response to continental ice mass variation. When water mass is transferred from ice sheets to oceans and vice versa, solid earth deforms to restore the isostatic equilibrium under a different surface loading setting. Solid Earth deformations and ice masses behave as density anomalies, thus affecting the vertical position of the mean sea surface, which is an equipotential surface of gravity (geoid). GIA is responsible for regionally varying relative sea level changes that are modulated in time with the viscous flow of mantle material (Peltier, 2004; Lambeck et al., 2004, 2011; Antonioli et al., 2020). Sea-level change along the Italian coast is the sum of eustatic, glacio-hydro-isostatic, and tectonic factors. The first is global and time-dependent while the latter two vary with location. The glacio-hydro-isostatic component exhibits a well-defined pattern and is readily predictable whereas the tectonic component exhibits a less regular pattern that is generally of shorter wavelength and less predictable (Lambeck et al., 2004).

In tectonically stable areas of the Mediterranean Sea, FTNs (of MIS 5.5 age) are typically found at elevations between 2 and 11 m above present sea level (Ferranti et al., 2006; Lambeck et al., 2011; Antonioli et al., 2018; Antonioli et al., 2023b). The base of the FTN is considered a reliable proxy for the mean paleo sea level, as its formation is closely tied to the local tidal range, making it a precise indicator of past sea levels (Antonioli et al., 2015; Fig. 2).

The age of FTN can be constrained through topographic correlation with adjacent marine deposits dated using the Th/U method or contain *Thetystrombus latus* (*Gmelin, 1791*, ex *Strombus Bubonius*) or the "Senegalese" fauna. This fauna consists of a fossiliferous association composed of gastropods and lamellibranchs now living along the coasts of Senegal, which entered the Mediterranean Sea during MIS 5.5. Subsequently, with the absence of the warm climatic conditions that had occurred between 132 and 116 thousand years ago (Shackleton et al., 2003), almost all these organisms in the Mediterranean Sea became extinct. Among all these fossils, also called "warm hosts", we remember: *Strombus bubonius* (today *Persistrombus latus*), *Cantharus viverratus*, *Conus Textudinarius*, *Mytilus Senegalensis*, *Mamilla lacteal*.

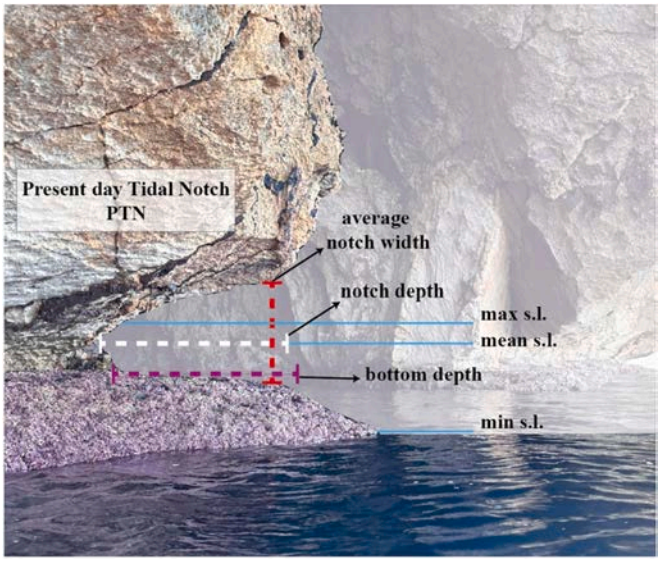

Fig. 2. Acquired micro-geomorphometric parameters of the surveyed tidal notches. The showed nomenclature follows the one proposed by Antonioli et al., 2015.

The Mediterranean Sea coasts, characterized by a microtidal regime with an average tidal range of around 40 cm, host numerous examples of late Holocene tidal notches formed in carbonate bedrock (Benac et al., 2004, 2008; Furlani et al., 2011; Furlani et al., 2014b; Antonioli et al., 2017). In Antonioli et al. (2018), the width of the PTN is compared with the fossil one in some particularly conservative areas (Gulf of Orosei or Capo Caccia and others): the TN width is entirely comparable; this means that the tide was the same. Therefore, because the tide during MIS 5.5 remained (in Mediterranean sea) the same as the present one, the relationship between tidal notches and sea level elevation can be discussed and estimates of MIS 5.5 sea level to be assessed and corrected. Several studies have identified and dated hundreds of Last Interglacial, or 'Tyrrhenian' (as littoral deposits related to MIS 5.5 are usually named in Italian nomenclature), sites throughout the Mediterranean (Blanc, 1936; Malatesta, 1985; Hearty, 1986; Hearty and Dai Pra, 1987; Zazo et al., 1999; Lambeck and Bard, 2000; Nisi et al., 2003). Using a compilation of 246 sites, all attributed to the MIS 5.5, Ferranti et al. (2006) and Antonioli et al. (2023a) found on 470 sites a significant alongshore difference in elevation from +175 to −125 m with respect to the present sea level, which they attributed to the interplay of regional and local tectonic processes, including faulting and volcanic deformation and partially for GIA.

2. Geological setting

The Sicilian Fold and Thrust Belt (SFTB) is a complex stack of double-verging thrust sheets with ENE-WSW direction that represent a segment of the Apennine-Tyrrhenian orogenic System, developed during the Cenozoic along the Africa-Europe plate boundary (Fig. 1). This complex thrust wedge, locally more than 20 km thick, is formed by deep-water Meso-Cenozoic carbonate units, overriding a more than ten km-thick carbonate platform, is characterized by a multi-stage tectonic evolution during the last 15 My evolving from thin to thick-skinned structural style (Catalano et al., 2013a; Gasparo Morticelli et al., 2015; Parrino et al., 2019; Sulli et al., 2021a, Todaro et al., 2022).

The study area lies in the northern sector of the Palermo Mts.

(Fig. 1A), where the Mesozoic carbonate platform succession pertaining to the Panormide paleogeographic domain extensively crops out. The outcropping succession represents a portion of a tectonic unit belonging to the Sicilian Fold and Thrust Belt, which displays SW-ward tectonic transport in this sector. In detail, the study area is the sea cliff, which, following a straight NNW-SSE trend, eastward bounds the Castellammare Gulf (Fig. 1), the more expansive bay along the northwest Sicily coast. The bay is hosted in a morpho-structural low elongated in approximately N-S direction perpendicular to the trend of the North-Sicilian margin, which borders south of the Tyrrhenian Sea (Fig. 1B).

Within this morpho-structural low, a clastic sedimentary succession, datable to the Plio-Quaternary based on the interpretation of seismic reflection data (Agate et al., 2005), has accumulated up to about 1000 m thick. Currently, the succession is mainly submerged at the continental shelf and upper slope and partly outcrops in the coastal areas south of the gulf, where it is found to consist of whitish marly limestones and

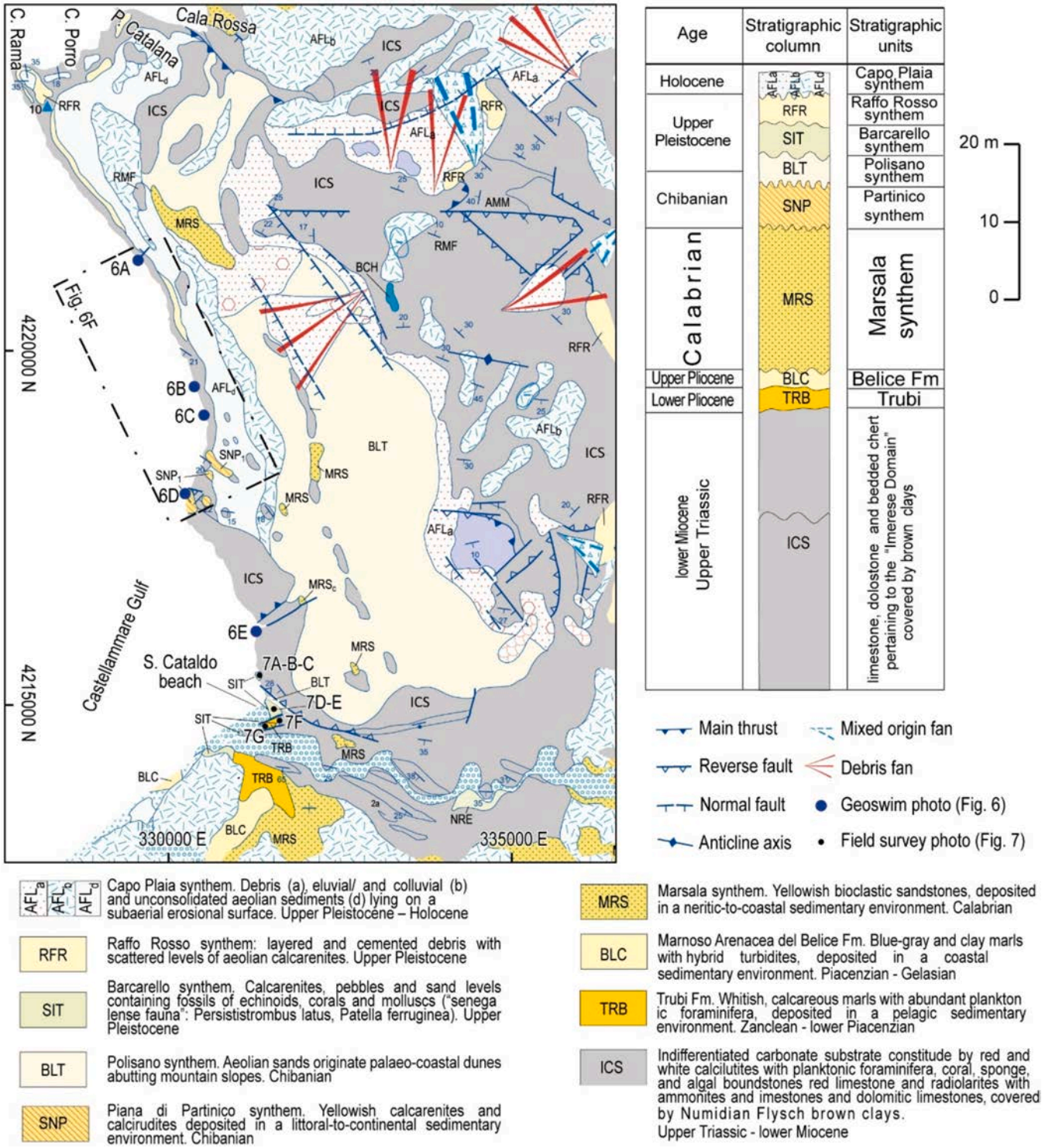

Fig. 3. On the upper left, the geological map of the surveyed area is represented at the scale of 1:50000 (modified from Catalano et al., 2013b). The map is co-ordinated with an accompanying stratigraphic column located at the top right and by its legend (in the bottom). Additionally, the map highlights the locations of the swim and field surveys, further illustrated in Figs. 6 and 7, respectively.

greyish marly clays of Pliocene age, transitioning upward to richly fossiliferous yellowish calcarenites and silt-sands with thin intercalations of conglomerates (Pleistocene age). Stratigraphic (Mauz et al., 1997) and seismostratigraphic studies (Catalano et al., 2013a) have recognized that Plio-Pleistocene succession is affected by unconformity surfaces related to sea level change and tectonics, along with faults with slight offset.

The investigated plunging cliff, NNW-SSE oriented, has a length of approximately 9 km and a height of up to 36 m a.s.l. and, is shaped in a Meso-Cenozoic sedimentary succession, made up of carbonate platform limestones and dolomitic limestones, upwards evolving to calcarenites and calcirudites deposited in carbonate platform margin environment, in turn passing to planktonic foraminifera bearing pelagic calcilutites; these carbonate deposits are topped by Tertiary terrigenous clays and sandstones (FYN, Fig. 3):

Upwards, the Meso-Cenozoic succession (ICS) is truncated by an enhanced unconformity, on which a Pliocene sedimentary succession unconformably lies, that is made up, from the bottom, by planktonic foraminifera bearing pelagic chalk (Lower Pliocene; TRB), upwards evolving to marls and silty clays (Upper Pliocene; BLC), above which a marine to continental Quaternary succession unconformably lies, that is formed by the following sedimentary unconformity-bounded stratigraphic units (Fig. 3):

- Marsala synthem (MRS): bioclastic sandstones (Calabrian age);
- Piana di Partinico synthem (SNP): yellowish calcarenites and calcirudites with fossil remnants of bivalves and gastropods, sands and reddish silts, lying on terraced, marine abrasion surface and deposited in a littoral-to-continental sedimentary environment (Chibanian age);
- Polisano synthem (BLT): quartz-carbonate aeolian sands (Chibanian age);
- Barcarello synthem (SIT): bioclastic calcarenites, pebbles and sands (upper Pleistocene age);
- Raffo Rosso synthem (RFR): debris with levels of aeolianites (upper Pleistocene age);
- Capo Plaia synthem (AFL): (*d*) unconsolidated aeolian sediments; (*b*) and eluvial/colluvial; (*a*) and debris (upper Pleistocene – Holocene age).

The sedimentary rocks of the different Pleistocene synthems outcrop in scattered deposits distributed along a broad plain at the top of the sea cliff, landward bounded by a continuous belt of recent slope debris pertaining to the Capo Plaia synthem.

During the Late Miocene – Early Pliocene, the Meso-Cenozoic carbonate-to-terrigenous succession was intensely deformed and shortened by compressional tectonics with the formation of faults and folds, which are also clearly visible along the Cape Rama cliff. Subsequently, the study area was affected by more recent (Pleistocene) compressive to transpressive high-angle faults with N-ward tectonic transport (Mauz et al., 1997; Catalano et al., 2013a; Sulli et al., 2021a, 2021b; Maiorana et al., 2024).

The coastline bordering the Castellammare Gulf to the south (Fig. 3) is a low, depositional coastline that accommodates an extensive sandy shoreline with a well-developed coastal dune system, except for very short stretches characterized by low cliffs (no more than 20 m high) shaped in calcarenite rocks of Pleistocene age (Marsala synthem and Piana di Partinico synthem). Along the coast, scattered patches of littoral deposits outcrop at the top of the low elevations located at the inner edge of the backshore; they consist of calcarenites, pebbles and sand levels containing fossils of echinoids, corals, and molluscs ("senegalense fauna": *Thetystrombus latus*, *Patella ferruginea*), pertaining to the Barcarello synthem (SIT).

The current stress field in place in the area, is hypothesized to have initiated around 0.8 million years ago (at the end of Calabrian age), when a significant tectonic reorganization occurred along the convergent Nubia-Eurasia margin in the central Mediterranean, driven by the lithospheric collision between Africa and Eurasia occurred (Goes et al., 2004; Billi et al., 2007; Sulli et al., 2019; Zitellini et al., 2020; Ferranti et al., 2021; Sulli et al., 2021a). The current GNSS velocity field illustrates this ongoing shortening, suggesting a roughly NNW-SSE-oriented Africa-Eurasia convergence at a rate of about 1 mm/yr (Ferranti et al., 2008; Mastrolembo Ventura et al., 2014; Devoti et al., 2017). Well breakouts further substantiate this kinematic framework, mapped active faults, and seismological data (Heidbach et al., 2018; Mariucci and Montone, 2020).

Seismic catalogues indicate that the study area experiences low to moderate seismicity, with a few significant earthquakes exceeding Mw 5.5. Notable events include the Mw 5.5 earthquake in 1726, the Mw 5.8 in 1823, and the Mw 5.9 in 2002 (Rovida et al., 2020). These seismic events predominantly occurred offshore in the southern Tyrrhenian Sea, a region where recent seismic activity is attributed to compressional and transpressional seismogenic sources (Anderson and Jackson, 1987; DISS Working Group, 2015; Pondrelli et al., 2020). This seismic pattern underscores the ongoing geodynamic interaction between the African and Eurasian plates and its impact on the region's seismicity.

3. Material and methods

The following sections comprehensively details the methodologies employed in the research design of this study. It explains how the land-to-sea surveys conducted within the study area were complemented by morphometric investigations, followed by an inversion approach applied to the morphotectonic data collected in the present study and from literature.

3.1. The offshore survey

Capo Rama was surveyed using the Geoswim approach firstly described by Furlani (2020). As described by Furlani and Antonioli (2023), more than 500 km of rocky coasts in the Mediterranean area have been surveyed using this approach. It collects observational and instrumental data at the intertidal and nearshore zone along large sectors of rocky coasts, mainly plunging cliffs, such as Capo Rama.

The surveys were carried out using a specially built raft (ISR, Fig. 4) to support the swim surveying activities along the coast and to host the instruments, such as GPS, cameras, and echosounders (Furlani, 2020). The ISR is 1.15 m long, 0.57 m wide, and 0.13 m high, and a net weight of 3 kg. It was made about 0.98 g/cm^3 of ethylene-vinyl acetate (EVA)—a light polymer resistant to UV. It is certified to be unsinkable by the producers (Sporasub). The raft was modified by adding L-section aluminium bars fixed from bow to stern above and below the raft, to permit the housing of the instruments (Fig. 4A, B). A set of cable holders fix the instruments on the IST to prevent loss of instruments. An aluminium roll bar was set on the stern of the raft. In the bow there was also a scuba gear dive flag for the safety of surveyors. The raft was usually pushed by swimming during the surveying activities. One camera has been set in waterproof housings and allow for the collection of ongoing videos and time-lapse images of the coastline being surveyed, both above and below the waterline (Fig. 4B). Different settings of cameras were adopted during the expeditions for the collection of videos or images as needed. The cameras were set laterally with respect to the raft to collect time-lapse images every second in the direction of navigation. The cameras set below the waterline included a TELESIN plastic dome 6 in. in diameter for superior optical performance in the seawater (Fig. 4D). The raft could also support waterproof LED lamps for the surveys within sea caves. Moreover, 3D models of sea caves can be collected using iPhone Lidar (Fig. 4C). A radio and an additional GPS were also used during the surveys.

The survey followed pre-planned routes at 1 m to 5 m from the coastline to identify the lateral variations in coastal landforms. Small changes in the route could occur with respect to the planned route due to

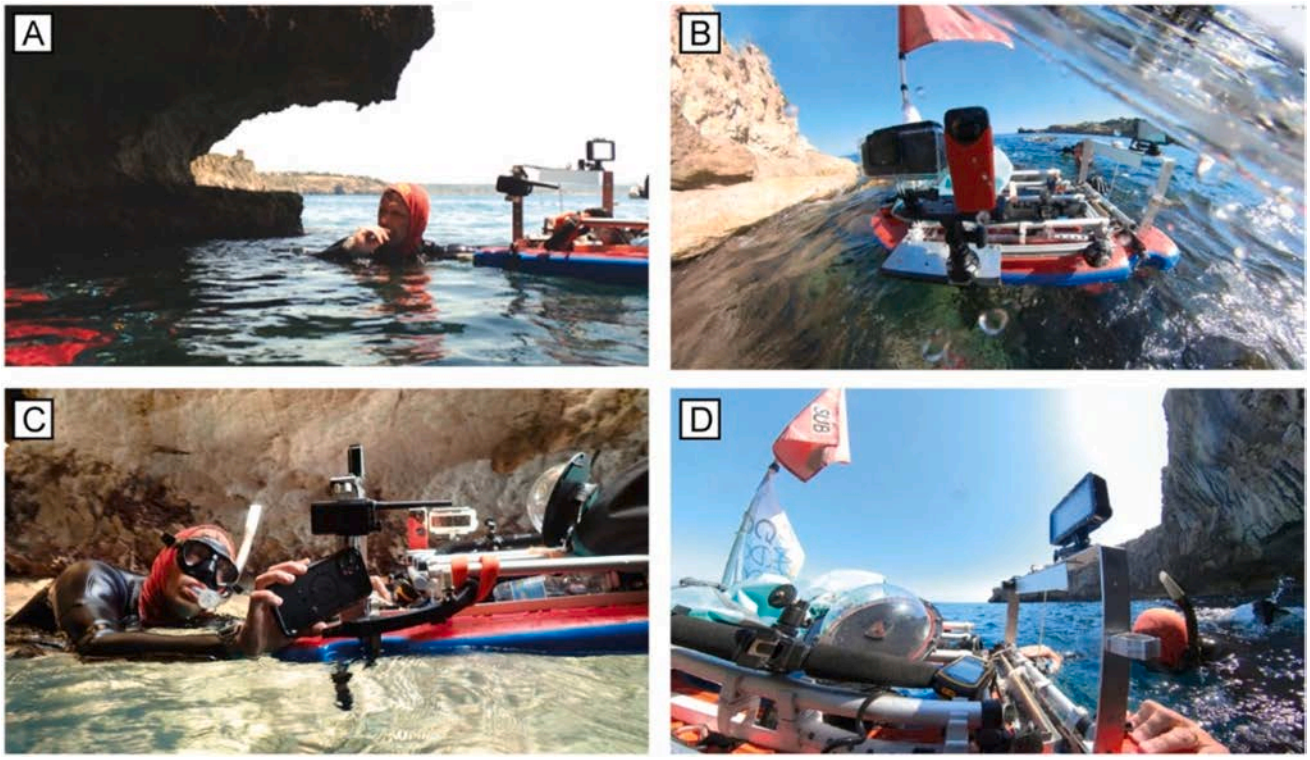

Fig. 4. The Instrumental Supported Raft (ISR) used for the swim surveys. A) Visual observations at a PTN; B) cameras set on the ISR; C) acquisition of images with an iPhone camera; D) navigation along sea cliffs at Capo Rama with the ISR.

the local changes in topography or due to variations in the sea conditions. The latter could force the swimmers to move out from the coast for safety reasons. However, sea conditions were calm, with no wind and waves. The navigation proceeded at a constant speed, ranging between 1 and 2 km/h, unless the swimmers encountered topographical obstacles or prominent geomorphological features.

One or more cameras can be set in waterproof housings and permit the collection of videos and time-lapse images of the sea cliffs, both above and below the waterline (Fig. 4C). The cameras should be set laterally concerning the raft to collect time-lapse images every second normal to the direction of navigation. The cameras set below the waterline include a plastic dome 6 in. in diameter to perform with higher optical performance in the seawater (Fig. 4C). A radio was used to communicate with the support vessel.

To acquire morphometric parameters of PTNs and FTNs, the approach proposed by Antonioli et al. (2015) was followed. According to this method, the micro-morphology of tidal notches is described by measuring three lengths: notch width, depth, bottom depth and bottom depth elevation (see Fig. 2 for further details). These measurements were analyzed alongside other data from the literature related to the study area and its immediate surroundings (Antonioli et al., 2018; Furlani et al., 2021). The "bottom depth elevation" data, as mentioned in Section 1.1, represent a proxy for the average sea level elevation. These data were considered alongside the elevations of the inner edges of the marine terraces to assign an age to them using a topographic correlation-based approach.

3.2. Morphometric analyses

We performed the morphometric analyses using a 2-meter geometrical resolution Digital Terrain Model (DTM) with a vertical accuracy of roughly 0.15 m. This DTM was acquired from Regione Siciliana through an aerial platform using a Leica ALS50 LiDAR system (Regione Siciliana, 2010).

Employing the *TerraceM* method (Jara-Muñoz et al., 2019), we performed the morphometric analyses aimed at identifying paleoshoreline angle locations via swath profiles traced approximately perpendicular to the coastline and covering most of the study area (Fig. 5). In alignment with the acquisition and validation workflow proposed by Parrino et al. (2023) data validation was carried out via a multi-step procedure, firstly, by examining elevation and slope variations along topographic profiles along the direction of maximum slope. Additional validation of the dataset was achieved by correlating the identified inner edge locations and elevations, with the upper lithological boundaries of the Plio-Quaternary succession exposed within the study area (see Fig. 3). Google Earth satellite imagery was employed to cross-verify the identified shoreline angle locations against any anthropogenic areas, using the imagery publicly accessible at https://earth.google.com/web/.

The validated dataset of shoreline angle elevation was analyzed via a distribution chart, which plotted coastline position against elevation. This analysis aimed to improve data reliability and remove any remaining outliers. Employing an in-house developed semi-automatic geospatial model, each shoreline angle point was projected along the coastline. Subsequently, distances were computed from these projections to a predefined point at the study area's western boundary designated as the zero point along the coastline.

This approach generated a chart comparing along-coast distance with elevation to minimize potential perspective distortions in the distribution chart. Such distortions could be introduced by projecting each shoreline angle point along a line with a fixed latitude or longitude value. This resultant chart aided in validating paleoshoreline elevation outliers and allowed for evaluating lateral continuity in the detected terrace orders across the study area.

3.3. The onshore survey and literature review

We performed a thorough review of the literature aimed at identifying the presence and, where possible, estimating the age of geomorphological markers in the area that are relevant to the research.

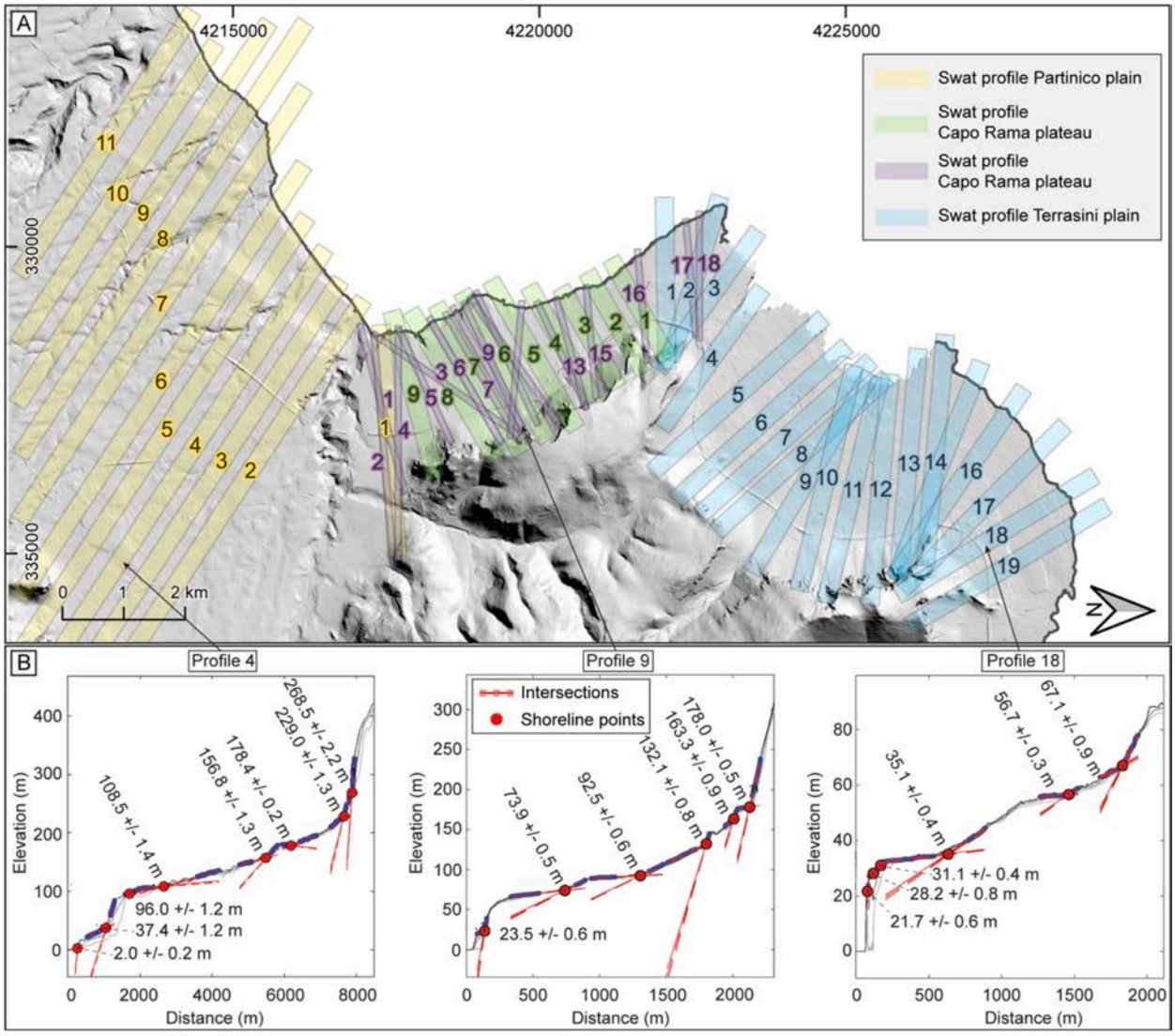

Fig. 5. A) The inset A show the map view of the four swath profile clusters employed for the morphometric exploration of the study area. The clusters are colour coded and are represented in yellow for the Partinico plain, in red and purple for the Capo Rama esplanade, and in light blues for the Terrasini plain. B) The three swath profiles in the inset B represent the most representative topographic distribution in the three previously cited coastal sectors. The red dashed lines display the 95 % confidence boundary of the topographic regression used to discriminate the shoreline angle points (represented as red dots). See Jara-Muñoz et al. (2019) for more information on the methodology used.

Moreover, multiple ground truthing field survey campaigns were conducted in the spring and summer of 2023 across the Partinico and Terrasini plains and in the Capo Rama esplanade. These campaigns aimed to catalogue the detected outcrops' lithological, sedimentological, and fossiliferous features to validate paleo-shoreline recognized through the morphometric analysis. In addition, the stratigraphic architecture of these geological formations was systematically delineated. Field surveys were conducted, utilizing published topographic base maps at a 1:10,000 scale (Carta Tecnica Regionale, CTR, provided by Regione Siciliana at: https://www.sitr.regione.sicilia.it/cartografia/carta-tecnica-regionale).

3.4. The Morphometric Inversion

An in-house developed code has been implemented to invert the observed paleo-shoreline elevation and elevation differences. The code was developed in the MATLAB environment (mathworks.com) and based on the "*OKADA: Surface deformation due to a finite rectangular source*" freely available in the Beauducel's MATLAB repository (Beauducel, 2020; https://it.mathworks.com/matlabcentral/profile/authors/1195687). It focuses on constraining the geometrical, geographical, and behavioural parameters of a fault that could be responsible for the observed deformations. To achieve this, we followed the faults parameterization forth by the Italian Database of Individual Seismogenic Sources (DISS Working Group, 2015). Constrained parameters include the fault's strike, dip, length, width (measured along the fault plane), and the fault centroid's geographical 3D coordinates.

As input data we used the elevation of marine terraces inner edges and tidal notches normalized elevations and the implemented optimization strategy employed the Monte Carlo method to solve the nonlinear and underdetermined inverse problem of the fault parameter inversion (Mosegaard and Tarantola, 1995). This strategy is grounded in a methodology established by Parrino et al. (2022) and incorporates iterative forward modelling, based on the Okada equations (Okada, 1985), conducted under specific assumptions: 1) a fixed fault rake of 90° (sensu Aki and Richards, 2002) and, 2) the exclusion of tensile deformations. Subsequently, the best-fit fault model was determined through a systematic Root Mean Squared Error (RSME) analysis between the observed input data and modelled vertical deformations. Our workflow also yields a range of viable fault models that reach RSME

values less than 0.02 % among all generated models.

Finally, we computed the goodness of fit of the overall best-fit inverse model by subtracting the normalized elevations of shoreline angle points from the modelled vertical deformation values. This dataset features a distribution that ranges from −1 to 1. In this distribution, extreme values represent points where the model diverges significantly from field observations. Conversely, values approaching zero indicate points where the model closely aligns with empirical observations.

4. Results

This section presents the outcomes of the integrated land-to-sea surveys conducted in the study area, detailing the results of the morphometric analyses performed and the subsequent morphotectonic inversion process, which utilized these findings as input data.

4.1. The Capo Rama plunging cliffs

The northernmost sector of the cliff, approximately 800 m in length, extends from the Cala Rossa beach to Punta Catalana (see Fig. 3 for toponyms) with an NW-SE trend. This is characterized by a *lithophyllum* terrace, a PTN and sea caves mainly developed on minor fractures. The cliff continues for about 750 m up to Cala Porro with a NE-SW trend with a much more developed fracturing system, that produced many sea caves forming on these fractures. The cliff then continues for approximately 500 m with an NW-SE trend up to Capo Rama and, in this sector, sea caves develop mainly on fractures.

The cliff continues with an NNW-SSE trend for about 6 km up to the San Cataldo beach. This entire stretch of the cliff is characterized by highly developed fracture and fault systems with several sea caves that lie on them. Pocket beaches and freshwater springs can also be identified, and the PTN shows a discontinuous trend with stretches in which it is absent or slightly carved and stretches in which it is well-formed. The most prominent landform in this sector of the cliff is an emerged FTN, whose height at its maximum depth was used as a proxy value to infer the sea level (please refer to Tidal Notch Width and mean sea level in Fig. 2). It outcrops all along the surveyed cliff, but its bottom depth elevation was measured at five points where the outcrop allowed for accurate measurement. The height varies from 1.9 m to 15 m (Fig. 6A–E) in the southernmost sector, near San Cataldo beach.

Together with the bottom depth elevation a set of tidal notches morphometric parameters were acquired and combined with those from relevant literature for the same area, the overall dataset main statistics be described as follows:

- TN Width (m): The notch width ranges from 0.37 to 0.52, with an average value of 0.445 and a standard deviation of 0.38.
- TN Depth (m): The notch depth varies between 0.65 and 0.220, with an average depth of 0.1196 and a standard deviation of 0.401.
- Bottom Depth (m): The bottom depth of the notch ranges from 0.18 to 0.139, with an average of 0.709 and a standard deviation of 0.279.

Using the same approach, the differences in morphometric parameters between PTNs and FTNs were calculated as follows:

- TN Width (m): The differences range from 0.05 to 0.3, with an average value of 0.2 and a standard deviation of 0.1.
- TN Depth (m): The differences range from −0.2 to 0.3, with an average value of 0.1 and a standard deviation of 0.2.
- Bottom Depth (m): The differences range from −0.79 to 0.1, with an average of −0.2 and a standard deviation of 0.4.

4.2. The sedimentary markers in the outcrop

The Capo Rama coastal cliff is topped by a *rasa* of roughly 9 km^2, 6.5 km long and 1.6 km wide with a great visual impact between the steep sides of the mountain (about 600 m high) and the cliff overlooking the sea. The plain shows a slight northward dip, with a difference in elevation between the southern and northern sectors of about 61 m (from 88 m to 27 m along a N-S profile; Fig. 6I), and with a slope of approximately 1.37 %. The difference in elevation on the E-W profile is 150 m (from 175 and 25 m; see Fig. 6H) with a slope of approximately 8.3 %.

This *rasa* has been interpreted as a shore platform of polygenic origin which is the result of multiple erosion cycles related to Quaternary subsequent shoreline transgressions and regressions. Similar polyphasic shore platforms are present in Sicily and were described by Ruggieri and Unti (1974) at elevations between 70 and 200 m.

In the study area, the pre-Quaternary deformed bedrock is unconformably overlain by littoral and continental deposits surveyed in small, scattered outcrops of limited thickness (Figs. 2 and 7). We have focused our investigation on the upper Pleistocene littoral deposits (Barcarello synthem). Despite their limited thickness in the study area, these deposits exhibit a notable variation in their nature, characterized by different facies. This diversity is particularly evident in the section of the cliff that extends from the Partinico plain to the Grotta delle Colombe (Fig. 7A). Some of these deposits are composed of oligomictic orthoconglomerates; key characteristics of these deposits include a reddish sandy matrix, low degree of sorting, angular clasts, and a low sphericity suggesting a high energy depositional environment, where the material was deposited with minimal transport (Fig. 7B and C). Some other littoral deposits are composed of parallel- or cross-laminated sand levels (Fig. 7D). In the southern sector of the Capo Rama cliff, most of these deposits are exposed and display features indicative of depositional paleo-environments typical of pocket beaches. These characteristics are illustrated in Fig. 7B–D.

Additionally, these littoral deposits are also found at the mouth of the Nocella River, where they have been carved into Pliocene deposits, a finding noted by Mauz et al. in 1997. Accompanying these terrace deposits, consisting of pebbles passing upwards to carbonate- and quartz-sand levels, are notable clusters of *lithophaga* holes in the bedrock, and shell fragments from bivalves and gastropods featuring a notable presence of *Senegalese fauna* (Fig. 7E–G).

As a combined result of literature results and the onshore surveys, a list of locations was produced where evidence of a paleo sea level, reasonably attributable to MIS 5.5, was identified. Please see Table 1 for a detailed list of these outcrops and their characteristics.

4.3. The fossil marine terraces

The study incorporates 57 swath profiles that can be broadly clustered into three distinct orientations and regions (Fig. 5). Specifically, 19 profiles are oriented roughly in the NW-SE direction and traverse to the Terrasini plain, while 27 are aligned in the NE-SW direction and follow the Capo Rama plateau. The remaining 11 profiles are oriented in an NW-SE direction and cover the Partinico Plain (Fig. 5). We explored a surface of approximately 90 km^2 in the study area through swath profile analyses. Notably, the highest density of swath profiles, and consequently the highest spatial resolution of the results, was computed in the Capo Rama plateau. Such high density can be justified because it is the summit plateau of the investigated crag and exhibited the most considerable variability in the elevations of the extracted shoreline angle points.

The swath profiles generated 319 shoreline angle points, yielding a sampling density of one point per roughly 3.5 km^2. The distribution of these points varied across the study areas: 79 points in the Terrasini Plain, 158 in the Capo Rama plateau, and 82 in the Partinico Plain. Of the initial 319 points, only 176 successfully passed multiple validation stages. It was considered reliable, among which 41 were detected in the Terrasini plain, 89 in the Capo Rama esplanade and 46 in the Partinico plain (Fig. 8). We also improved this dataset through additional points discriminated from field surveys.

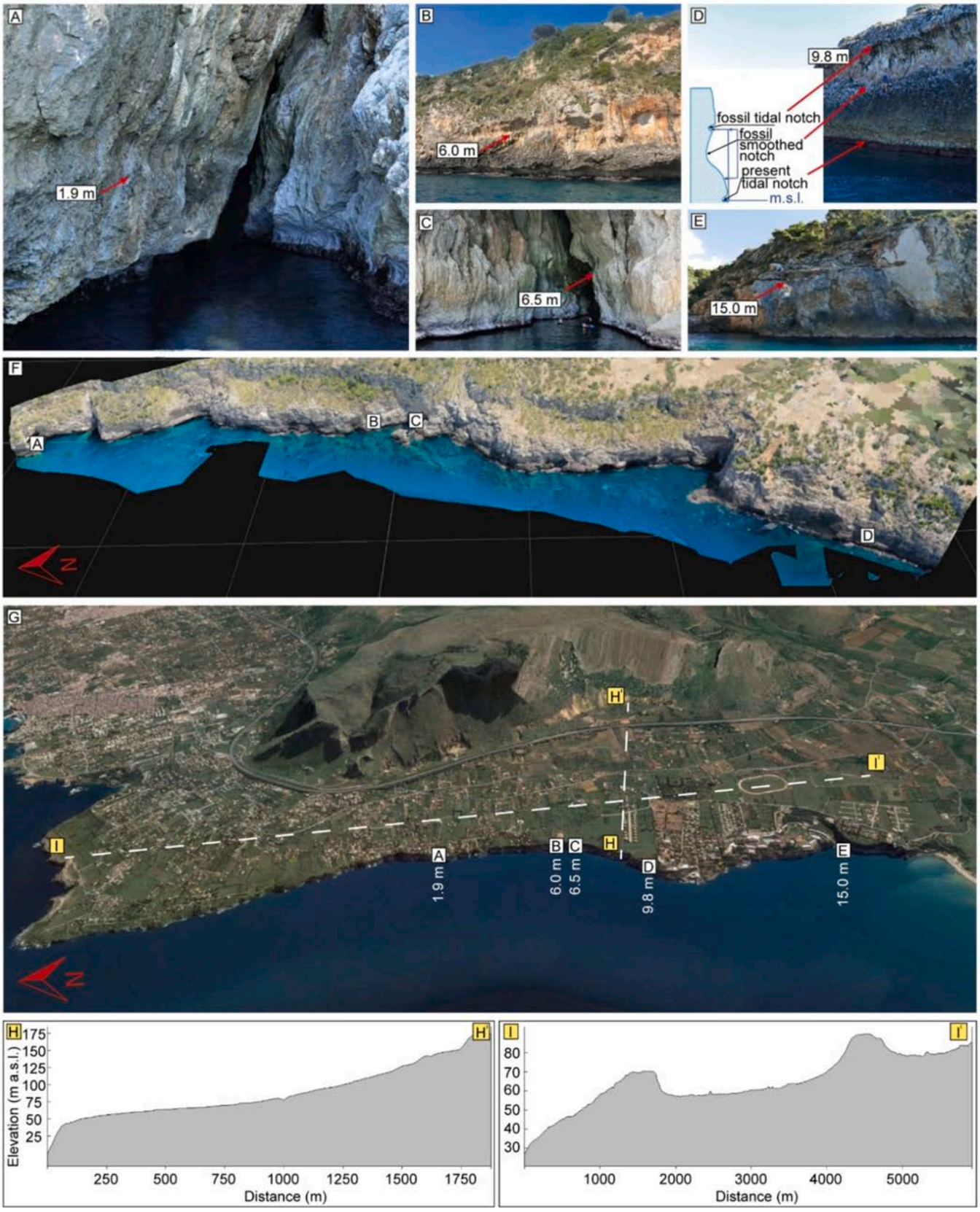

Fig. 6. Detailed visual documentation of the FTN surveyed along the Capo Rama plunging cliff: Insets labelled from A to E display the FTN at various elevations observed in the NNW-SSE portion of the Capo Rama cliff. Additionally, inset F features a 3D photogrammetric reconstruction of the Capo Rama cliff providing a comprehensive view of the cliff's topography and shape; inset G represents a 3D Google Earth view of the study area which shows the position of the tilted FTNs and the traces of 2 topographic profiles, H-HI and I-II, whose trend is shown in the lower part of the figure.

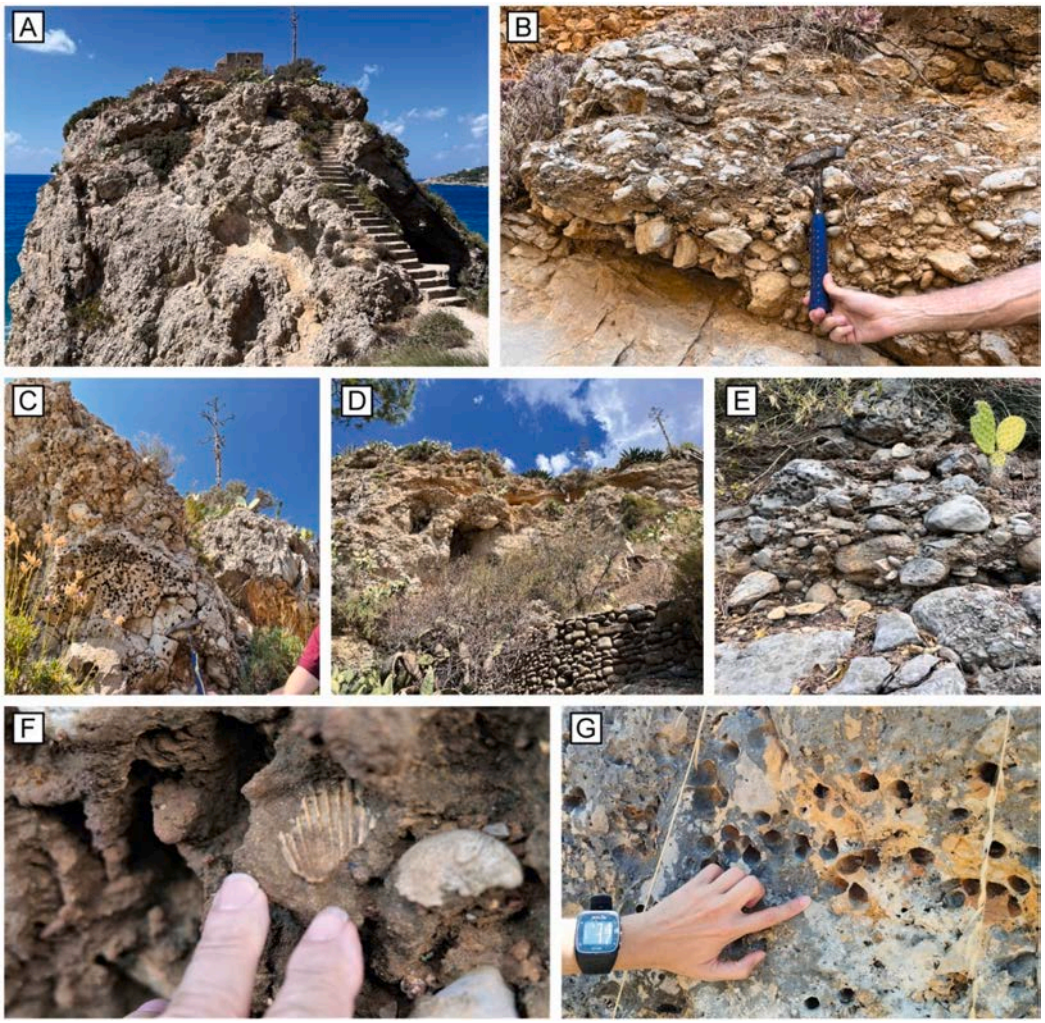

Fig. 7. A) Displays a panoramic view of the Grotta delle Colombe outcrop site; B) and C) Present detailed views of the oligomictic orthoconglomerates outcropping along the cliff. These views are focused specifically on the stretch between the Partinico plain and the Grotta delle Colombe study site, highlighting the textural and compositional characteristics of these conglomerates; D) Panoramic view of a marine sandstone deposit; E) Lithophaga holes carved into the conglomerate outcrops; F) Features a fragment of thick-shelled bivalves, which are interpreted to be part of the Senegalense fauna, providing evidence of the area's paleontological history; G) Depicts lithophaga holes bored into the pre-Quaternary deformed carbonate bedrock (see Fig. 3 for location of pictures A-G).

To reconstruct the spatial distribution of paleo-shorelines, the envelope of the shoreline angle points was delineated across the entire study area. This process revealed those paleo-shoreline differential numbers across the three plains of interest. Specifically, six paleo-shorelines were observed in the Terrasini Plain, seven in the Capo Rama plateau, and seven in the Partinico Plain, as delineated in Fig. 8. The identified paleo-shorelines exhibit varying spatial characteristics across the study regions. In the Capo Rama plateau, the horizontal distance measured between the various recognized paleo-shoreline is considerably smaller regarding the analogous observed distance in the other sectors. Conversely, in the Partinico Plain, the paleo-shorelines separate more wide terraces. We propose a systematic representation of elevational and slope data of the detected paleo-shorelines labelled through progressive letters (from *a* to *h*, see Figs. 8 and 9) starting with the lowest in elevation.

Table 2 presents data on elevation ranges and corresponding slopes for eight labelled paleoshorelines (ranging from '*a*' through '*h*', Figs. 8 and 9). The elevation ranges span from a minimum of 2 m to a maximum of 145 m asl, with slope values consistently negative, ranging from −0.18° to −0.07°. An analysis of the elevation ranges reveals a clear progression from lower to higher elevations across the detected paleo-shorelines. The lowest range is observed in the *a* (2–39 m), while the highest is in the paleoshoreline *h* (115–145 m). The steepest slope is found in paleoshoreline *a* at −0.18°, which corresponds to the lowest elevation range. In contrast, the gentlest slope of −0.07° is observed in paleoshorelines *e*, in the middle of the elevation sequence. Notably, areas *b*, *c*, *f*, and *g* exhibit identical or nearly identical slopes, ranging from −0.11° to −0.12°, despite their different elevation ranges.

4.4. The fault model

Table 3 summarizes the fault parameters computed through the morphotectonic inversion procedure. The results of this inversion consist of a best-fit model and a series of models that solve the inverse problem with a RMSE value less than 0.02#.

In the best-fit model, the fault centroid is located at a depth of 3 km, with coordinates E: 342500 and N: 4221000. The fault plane has a dip of 55° and a strike of 69°, with dimensions of 26 km and a width of 2.5 km.

The parameters exhibit minor variations in the top 0.02# RMSE of models with a minimal observed-to-modelled misfit. The depth remains consistent at 3 km, and the dip stays at 55°. Coordinates E and N stay approximately around $3.43 * 10^5$ and $4.22 * 10^6$, respectively. The strike varies slightly between 69 and 70°, while the length fluctuates between 26 and 26.1 km. The width ranges from 2.5 to 2.9 km. The maximum

Table 1
This table includes all the relative sea levels (RSL) indicators outcropping in the area. Site 11 elevation modified after Mauz et al., 1997; this study. Site 1 references: Fabiani, 1941; Bordoni and Valensise, 1999; Ferranti et al., 2006; Cappadonia et al., 2020. Site 2 references: Foglio Geologico Palermo 595 Sintema Barcarello, Gignoux, 1913. Site 4 and 5 references: Carta Geologica d'Italia, Foglio Partinico 594. Site 11, 12 references: Mauz et al., 1997. Ispra: Carta Geologica d'Italia, Foglio Partinico 594 and Carta Geologica d'Italia, Foglio Castellamare del Golfo 593. Site 3, 6, 7, 8, 9, 10, 13 references: This paper.

Site ID	Lat/Lon	RSL indicator	Elevation (m asl)	MIS 5.5 Age marker
1	38.120628/ 13.364375	Fossil beach	10.0 ± 1.0	*Thetystrombus latus*
2	38.204951/ 13.280750	Fossil beach	2.0 ± 1.0	*Thetystrombus latus*
3	38.200524/ 13.270055	Lithophaga holes	2.0 ± 1.0	Topographic correlation
4	38.188216/ 13.130036	Fossil beach	1.5 ± 1.0	Topographic correlation
5	38.188456/ 13.103653	Fossil beach	1.5 ± 1.0	Topographic correlation
6	38.123590/ 13.065450	Tidal notch	1.9 ± 0.5	Topographic correlation
7	38.113150/ 13.071190	Tidal notch	6.0 ± 0.5	Topographic correlation
8	38.111150/ 13.072030	Tidal notch	6.5 ± 0.5	Topographic correlation
9	38.104560/ 13.070310	Tidal notch	9.8 ± 0.5	Topographic correlation
10	38.093670/ 13.077470	Tidal notch	15.0 ± 1.0	Topographic correlation
11	38.086624/ 13.078694	Fossil beach	11.0 ± 3.0	abs 131 ± 43
12	38.084273/ 13.074716	Fossil beach	18.0 ± 2.0	abs 101 ± 43

and minimum values of the parameters are also provided. The maximum values are a strike of 70°, a length of 26.1 km, and a width of 2.9 km. The minimum values consist of a strike of 69°, a length of 26 km, and a width of 2.5 m.

For the best-fit model, the calculated upper tip of the fault is at a depth of approximately 1215 m, while the detachment level is at approximately 4785 m. The depth parameters exhibit some variability in models' top 0.02# RMSE. Using the minimum width of 2.5 km, the upper tip is approximately 1.215 km, and the detachment level is approximately 4.785 km. Utilizing the maximum width of 2.9 km, the upper tip is approximately 929 m, and the detachment level extends to approximately 5.071 km.

The goodness-of-fit of the best-fit model reveals spatial heterogeneity in performance across the study area. As depicted in Fig. 10A, a substantial portion of the dataset, precisely 63 %, adheres to a 20 % error edge centred around zero (200 out of 319 points). A smaller segment, amounting to 35 %, falls within a 10 % error edge, as illustrated in Fig. 10B (112 out of 319 points). The skewness of the goodness-of-fit distribution is right-oriented, indicative of a general model tendency to underestimate vertical deformation.

Geographically, the model's performance varies across different sectors. In the Partinico Plain and Capo Rama Esplanade, lower error levels are predominantly observed in points near the coastline. In contrast, the Terrasini Plain exhibits a distinct NW-SE elongated area where the model consistently overestimates vertical deformation. The model frequently underestimates vertical deformation on the slopes of the reliefs and in the more inland portions of the Partinico Plain (refer to Fig. 10).

5. Discussions

Considering the joint use of tidal notches and marine terraces we argue the achieved outcomes in the framework of the late Quaternary tectonic deformation recorded in the investigated coastal belt.

5.1. On the joint use of tidal notches and inner edge

The handled study case facilitated an evaluation of the joint use of FTN and FMT as geomorphological markers. This allowed focussing on their combined utility and limitations for coastal tectonic investigations. This kind of study aims to use these markers as paleo-geodetic indicators and temporal benchmarks through a multidisciplinary on-offshore approach. However, it is important to emphasize that this approach is valid and can be replicated only in regions with similar tide ranges (e.g., the Mediterranean area, southern India, northern Chile; Rosendahl Appelquist, 2012) and not in areas characterized by low differential vertical movement rates and high tide ranges, such as large portions of the Atlantic European coast, Alaska, northwestern Australia, or southern Argentina (Archer, 2013).

The surveying and mapping of FTN and FMT are characterized by differing difficulty levels, with one generally considered more challenging than the other. Acquiring data about TN, which are features of outcropping cliffs or paleocliffs, necessitates specialized approaches, such as close-range remote sensing or coastal offshore surveys, which can be expensive and time-consuming. On the other hand, FMT can be easily detected with traditional field techniques and through modern morphometric approaches, even if they are subject to the issue of morphological convergence. This hampering factor arises when multiple geological processes contribute to the formation of staircased coastal features, thereby introducing potential inaccuracies in determining paleoshoreline elevations and spatial distribution (Castiglioni, 1979; Huggett and Shuttleworth, 2022).

The accuracy of geomorphological markers in representing mean sea level can vary. FTNs are considered the most precise proxies for paleocoastline elevations, providing centimetre-level accuracy in the Mediterranean Sea region (Vacchi et al., 2012; Antonioli et al., 2015; Lorscheid et al., 2017; Antonioli et al., 2018; Mauz et al., 2020;). In this regard, it is interesting to note that the dimensions of PTNs and FTNs are very similar, with a difference of about 0.2 m in TN width. This difference was attributed by Antonioli et al. (2018) to a combination of chemical-mechanical erosion of the carbonate bedrock and the current absence of the biological rim (*Vermetids*, *Corallinales algae*) in the FTN. It is possible to assert that, during the period related to MIS 5.5, the tidal range in the study area must have been like the current one.

In contrast, the accuracy of modern morphometric techniques for surveying FMT significantly depends on the available topographic dataset and, thus, on the spatial resolution of the Digital Elevation Models (DEMs) employed. On average, these techniques can achieve metric-level accuracy (Jara-Muñoz et al., 2019). Furthermore, the accuracy of using FMT as proxies for paleo-sea levels is further complicated by considerations of coastal onlap, a concept elaborated by Vail et al. (1977, 1984) and subsequently refined by (Catuneanu et al., 2009). The position of the inner edge of a FMT is intrinsically linked to the location of the coastal onlap, which is influenced by the prevailing depositional environment. Recognizing these intricate relationships is pivotal for enhancing both the accuracy and interpretive power of geomorphological markers in studies of coastal tectonics. In floodplain settings, the positioning of the coastal onlap slightly above the reference sea level can result in overestimating paleo-sea level elevations. This issue underscores the importance of corroborating morphometric findings with sedimentological investigations to validate the identified geomorphological markers.

As proxies for mean sea level, these markers simplify the representation of an equipotential surface at localized observation scales, offering consistent information about the elevation of this paleo-surface and its current geometry (Cheney, 2001; Eshagh, 2021, and references therein). Their elevation is crucial for assessing vertical displacements since their formation, while their spatial distribution is crucial for identifying deviations from assumed linearity or horizontality (Ramos

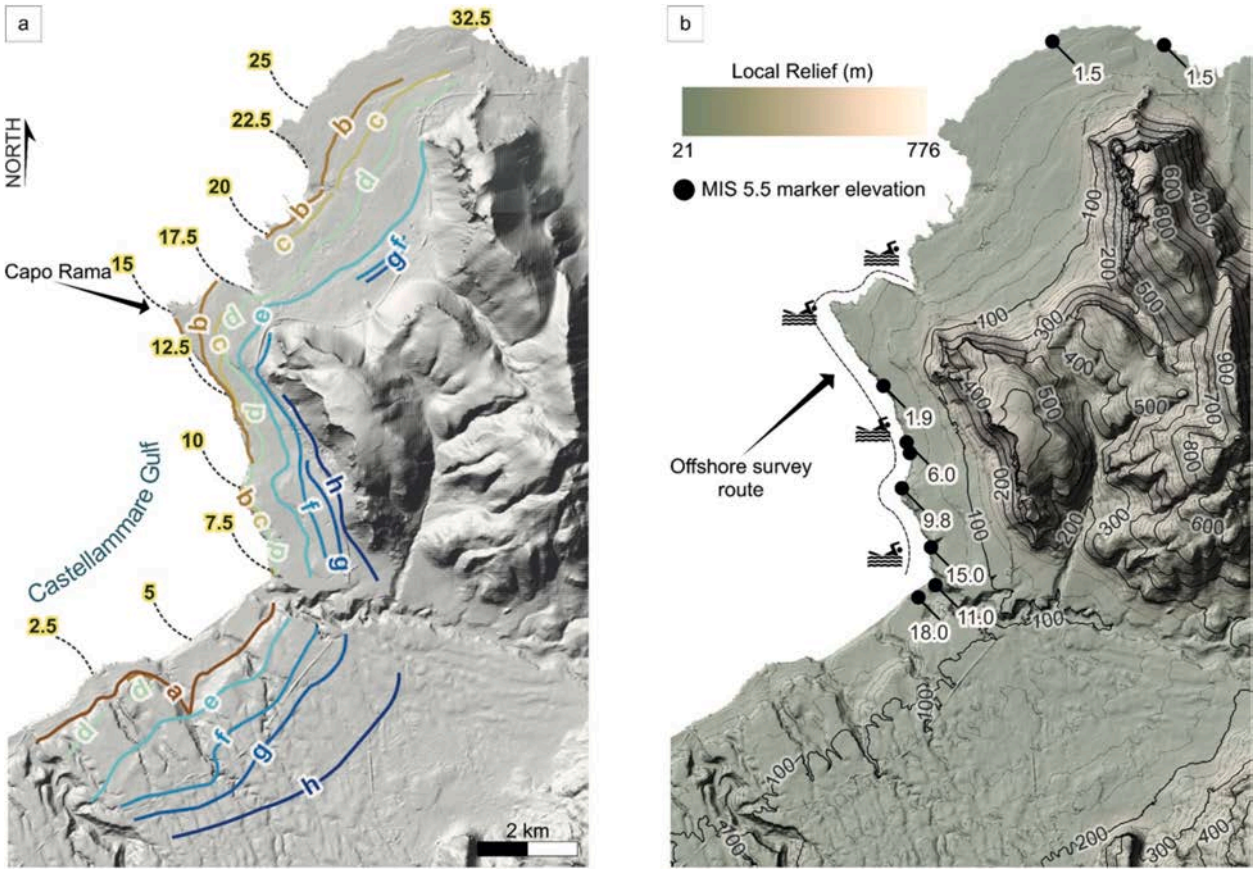

Fig. 8. a) The colour-coded polylines represent the result of interpolating the 8 extracted paleoshorelines in the study area. The white buffered letters represent the progressive letters (from a to h) assigned as labels to each detected paleoshoreline. The yellow buffered numbers along the coast represents the along-coast distance expressed in km. b) The colour coded DEM represent the Local Relief value computed through a circular moving window characterized by a radius of 1 km using the MATLAB library Topotoolbox (Schwanghart and Scherler, 2014). Black dashed line represents the offshore survey route. Black dots connected to white buffered numbers represent part of the literature data shown in Table 1 (from row 4 to 12). Thinner contour lines spacing is 20 m while thicker contours spacing is 100 m.

and Tsutsumi, 2010; Ramos et al., 2012; De Santis et al., 2021). Following the discussion on the critical role of altitude and spatial distribution of these geomorphological markers, it is essential to consider temporal aspects. The timescales involved in forming TN and shore platforms significantly diverge. PTN can be generated in as few as hundreds of years, providing relatively immediate indicators for vertical displacements (Furlani et al., 2009; Furlani and Cucchi, 2013; Antonioli et al., 2015).

Conversely, FMT require up to hundreds of thousands of years to form, posing challenges for their use as contemporaneous markers with FTN. This temporal difference can manifest as inconsistencies in areas with differential vertical motions. A single FMT could perfectly align with multiple periods represented by different FTN. The rate of these vertical motions further impacts the type of terraced surfaces formed—low rates generate large polycyclic terraces. In contrast, high rates yield classic staircased configurations (De Gelder et al., 2020). Given these complexities, these markers' elevation and spatial data must be interpreted carefully, factoring in the potential reoccupation of terraced surfaces and misleading low peaks in eustatic curves.

5.2. Age model attribution

The geomorphological markers age model attribution was based on available numerical dating from the literature and topographic correlations of the computed elevations (shown as points in Fig. 9). Using the Optically Stimulated Luminescence method, Mauz et al. (1997) determined a thermoluminescence age of 101 ± 43 and 131 ± 43 (kyr ± 1st standard deviation) for the calcarenite deposits outcropping at the location shown in photos 7G–7F (see top left panel of Fig. 3 and, sites 11 and 12 in Table 1) and interpreted them as having been deposited during MIS 5.5. It must be considered that the dated deposits consist of sediments from a submerged beach environment, and therefore their elevation cannot be regarded as a paleogeodetic marker.

These deposits outcrop at an elevation of about 11 and 18 m asl (Table 1) and based on the findings from the field survey conducted in this study, we identified that the submerged beach deposits in the elevation extend to 21 m asl. Additionally, we detected *Lithophaga* holes in the surrounding area on a small limestone paleo-cliff, reaching up to an elevation of 24 m asl. Finally, the closest inner edge was identified through morphometric analyses (and validated during the survey) in the slightly higher areas and lies at about 34 m asl (Fig. 8). The dated deposits are characterized by a high degree of spatial and topographic correlation with the southernmost detected FTN outcrop. Specifically, these outcrops are separated by an horizontal distance of approximately 400 m and an elevation difference of about 3–4 m. Such spatial and topographic correlation constitutes the primary reason leading us to assume that the detected FTNs can be attributed to the same MIS.

Another possible consideration regarding the attribution of the age model involves considering the elevation differentials of various eustatic peaks around the time frames of the considered dating to compare them with the elevation differences observed between the markers. Specifically, the elevation differential between MIS 3.3 and MIS 5.1 ranges from 24 to 2 m (Antonioli et al., 2021a, 2021b). Moreover, MIS 5.1 and 5.3, corrected for isostatic sea levels and spanning between −16 and −12 m, is approximately 8 m (Antonioli et al., 2021b, 2021c). In contrast, the differential between the eustatic MIS 5.5 elevation

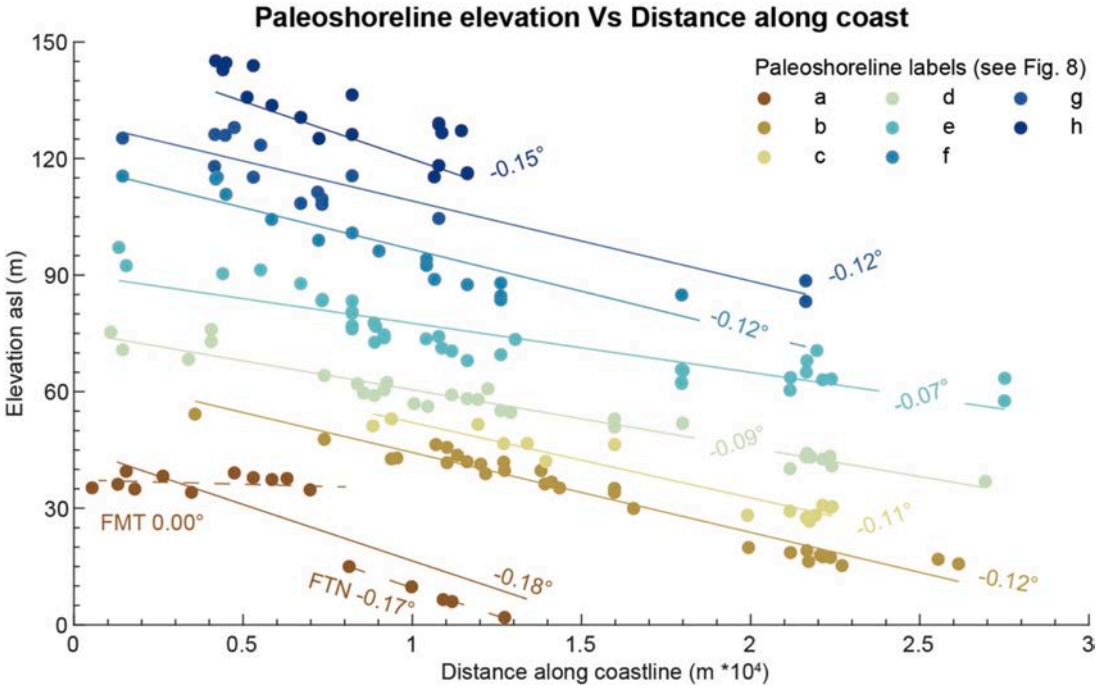

Fig. 9. Inner edges elevations against their elevation projected along the coastline. Colour-coding represents the different paleoshorelines as labelled and coloured in Fig. 8. Regression Lines are represented by solid-coloured lines for each detected inner edge illustrating the general slope of the inner edges along the coast. Superimposed on these regression lines are their slope values. The chart illustrates three regression lines for the paleoshoreline a, the dashed lines are for the FMT and one for the FTN points only, while the solid one represent the overall point population. Please see Section 5.2 for the age model attribution and Section 5.3 for some consideration on the different slope of the regression lines.

Table 2
This table presents elevation ranges (in meters above sea level) and associated slopes (in degrees) for eight detected paleo-shorelines labelled 'a' through 'h'.

Label	Elevation range (m asl)	Slope (°)
a	2–39	0.00/−0.17
b	15–54	−0.12
c	26–53	−0.11
d	36–76	−0.09
e	57–97	−0.07
f	83–118	−0.12
g	88–128	−0.12
h	115–145	−0.15

Table 3
This table includes: The best fit fault model parameters derived from the fault inversion process; The best 0.02 RMSE Parameters list the fault models that have achieved a Root Mean Square Error (RMSE) of 0.02 or lower; Minimum and maximum boundary parameters extracted from the models with the best 0.02 RMSE.

Depth (m)	Dip (°)	E	N	Strike (°)	Length (m)	Width (m)
Best fit						
3000	55	342,500	4,221,000	69	26,000	2500
Top 0.02 RMSE						
3000	55	3.43E+05	4.22E+06	69	26,000	2700
3000	55	3.43E+05	4.22E+06	69	26,100	2500
3000	55	3.43E+05	4.22E+06	70	26,100	2500
3000	55	3.43E+05	4.22E+06	70	26,000	2500
3000	55	3.43E+05	4.22E+06	69	26,000	2500
3000	55	3.43E+05	4.22E+06	70	26,000	2500
3000	55	3.43E+05	4.22E+06	70	26,000	2600
3000	55	3.43E+05	4.22E+06	69	26,000	2800
3000	55	3.43E+05	4.22E+06	70	26,100	2500
3000	55	3.43E+05	4.22E+06	70	26,000	2700
3000	55	3.43E+05	4.22E+06	69	26,000	2900
3000	55	3.43E+05	4.22E+06	69	26,100	2600
3000	55	3.43E+05	4.22E+06	69	26,000	2600
3000	55	3.43E+05	4.22E+06	69	26,100	2700
Max						
3000	55	3.43E+05	4.22E+06	70	26,100	2900
Min						
3000	55	3.43E+05	4.22E+06	69	26,000	2500

(corrected for isostasy) for the northwest coasts of Sicily, attributed to 8.4 m during the maximum transgression at 118 ka BP (Antonioli et al., 2018), is about 20 m. Similarly, the elevation differential between the MIS 5.5 elevation and MIS 7.1, 7.3, and 7.5 ranges from 20 to 26 m, considering that sea levels during those eustatic peaks fluctuated between −12 and −18 m at 195, 210, and 240 ka BP (Dutton et al., 2009).

Since the difference in elevation between the two morphometric markers (FTN at 15 m asl and the closest FMT at 34 m asl) is 19 m, it is possible to assert that this elevation difference fits elevation differences relative to the time intervals between: *a*) MIS 3.3 and 5.1; *b*) MIS 5.3 and 5.5; *c*) MIS 5.5 and 7.1. Considering this and considering both the previously described numerical dating and the elevation differences, the age model that best fits these parameters is the one that attributes the FTN and the lower detected FMT inner margin to an age between the last two eustatic peaks of MIS 5. To follow a conservative approach and avoid overestimating the consequent uplift rates, the age attributed in this study is that of MIS 5.5.

Considering what above, the age model attribution regarding the terraced surface atop the Capo Rama coastal cliff, was performed considered that: *a* - In its northern sector, the shore platform cuts through bioclastic arenites belonging to the lower Quaternary "Marsala synthem" (Figs. 3 and 6). *b* - On the shore platform at the top of the coastal cliff, narrow strips of coastal deposits outcrop, which belong to the Partinico and Polisano synthems of middle-upper Quaternary age

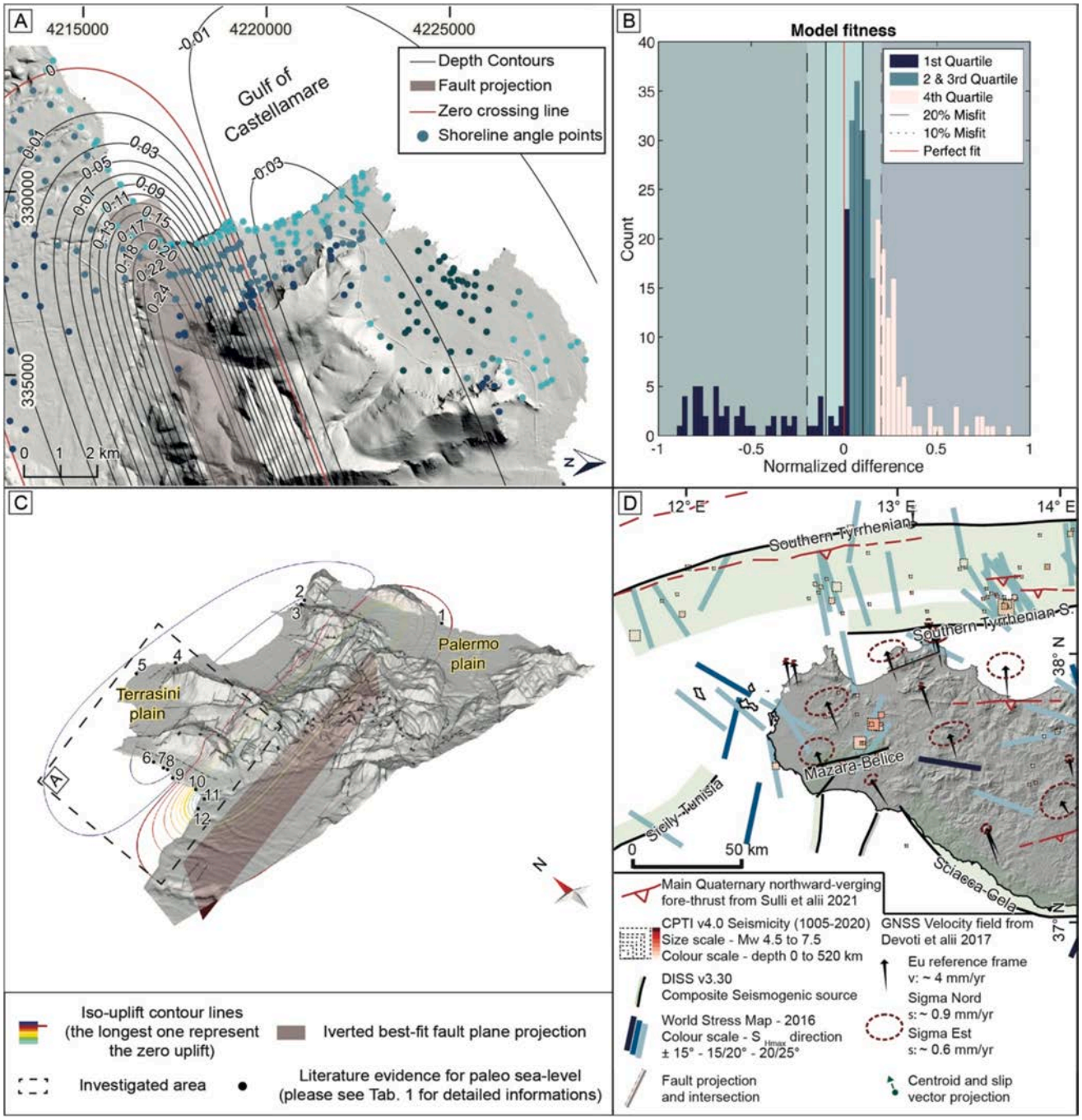

Fig. 10. Inset A show the map view of the vertical deformation computed through the fault deformation modelling of the inverted best fit fault model applying 1 m of slip along the fault plane. Solid black lines represent the deformation contours with superimposed the vertical deformation values expressed in meters. The red solid line represents the zero-crossing line delimitating the uplift area from the subsidence area. The transparent reddish polygon represents the plane projection of the best fit fault model. The colour-coded points represent the location of the paleo inner edge extracted. The colour code can be read in the background colours of the Model fitness histogram represented in the inset B. The red line in the inset B represent the location of the perfectly fitting points bin while the bin colour coding represents the quartile distribution of the computed data. Inset C represent the 3D view of the computed best fit model and the digital elevation model's hillshade is included, with the main tectonic structures of the area superimposed for context. Numbers from 1 to 12 refer to the sites in Table 1 and numbers in parentheses to paleo RSL elevations in meters. Black arrows in Inset D represent the GNSS velocity field as reported by Devoti et al., 2017, with dashed red ellipses indicating the confidence intervals of these measurements. The blue-graded lines illustrate the direction of maximum horizontal stress, based on data from the World Stress Map while, the squares of varying colours and sizes on the map represent the earthquakes recorded in the CPTI15 (INGV) database. The figure also includes the main Quaternary northward-verging fore-thrust as identified by Sulli et al., 2021a.

(Fig. 3). *c* - The uppermost Pleistocene littoral deposits, associated with the Barcarello synthem, are observed as perched outcrops along the coastal cliff but not at its top. Based on these observations, we hypothesize that the terraced surface atop the Capo Rama cliff was carved between 800 (the end of the deposition of the "Marsala synthem") and 200 ka BP. Consequently, the age model of the FMT inner margins detected in the Capo Rama rasa range from the MIS 7a to the MIS 11a.

5.3. New clues for the active tectonic framework

The research presented intersects with a complex array of existing literature, which collectively provides essential insights for understanding the puzzling seismotectonic framework of this sector of the NSCM. Notably, Vail et al. (1984) highlights the primary role of the NSCM in accommodating the Sicilian fault and thrust belt current shortening, which resonates with our results, highlighting the differential vertical displacements and spatial distribution of the analyzed geomorphic markers. This view gains further support from (Milia et al., 2018), who detect, in the near offshore of the Termini Imerese Basin (located along the NSCM some km eastward from the Castellammare Gulf), seaward inclined Quaternary depositional sequences as evidence of faults activity, block tilting and relative uplift. These findings are complemented by Parrino's work (2022, 2023), which brings attention to active blind faulting processes and re-emphasizes the need for re-evaluating the Quaternary uplift history in this sector of the NSCM. Such observations dovetail with structural models (Catalano et al., 2002; Albanese and Sulli, 2012; Catalano et al., 2013a), suggesting that blind thrust and reverse faulting may be involved in the area's deformation. Moreover, these authors propose detachment levels of these structures at depths compatible with the greater depth values described in Table 3.

The best-fit fault model inverted in this study (see Table 3) not only aligns coherently with the N-verging structures proposed in the outlined literature but also uncovers how the ongoing deformation from these tectonic structures is currently driving the landscape evolution. The validity of our best-fit fault model's deformation is also corroborated by the elevations of the MIS 5.5 markers shown in Table 1, all located within the region impacted by fault-induced deformation. Furthermore, it reveals morphotectonic evidence of uplift, as indicated by the different elevations of FMT' inner edges and FTN, challenging the notion of stability previously hypothesized in earlier literature. Particularly noteworthy is the evidence from the MIS 5.5, anand highstand event 8.4 m higher than the current level, occurred around between 127 and 117 ka years ago. Starting from the fossil tidal notches that we found at 1.9 m (the northern, see Fig. 6A), in all the marine caves visited in the S direction of the Capo Rama sea cliff, it has always been possible to observe fossil holes of Lithophaga at slightly lower altitudes than the five observed and measured FTN. Inside the caves located further north, starting from Cala Rossa, no Lithophaga holes are observed while carefully observing the internal walls. This confirms the hypothesis of a post-MIS 5.5 fault related tilting, which caused the altitude of the FTN to decrease in a northern direction until they disappeared below the sea (Cala Rossa).

The present elevation of the MIS 5.5 inner edge is approximately 34 m above sea level and allows an estimate of an uplift rate of around 0.22 mm/year. This rate is calculated near the zone of maximum uplift at which the model performs best and provides a crucial quantitative measure of the region's tectonic activity (as illustrated in Fig. 10). It is consistent with the order of magnitude of uplift rates proposed by Parrino et al. (2022, 2023). This value is roughly double the estimates by Ferranti et al. (2006). However, the latter study does not account for the immediately adjacent FMT inner edge, which is approximately 16 m higher. This discrepancy necessitates careful interpretation of sediment dating and uplift rates, as failing to recognize the inner edge leads to underestimating the uplift rates in the area. Nevertheless, it is important to state that even if the assumption made regarding the age model in the previous section should be poorly reliable, and thus, the geomorphological markers considered belong to earlier interglacial periods (such as MIS 7.1), this would not undermine the validity of the proposed tectonic modelling. In fact, the modelling is primarily based on the inversion of geometric, geographic, structural, and kinematic parameters of the fault plane, and not on the associated slip rates. In the inversion process, a slip of only 1 m was applied to the fault plane, and the deformation of the geomorphological markers was normalized to range from zero to one. In this sense, the uplift rates are calculated based on the age model and not on the inversion model. Moreover, the robustness of this inversion can be supported independently of the tidal notch data, as these represent only a small portion of the dataset used for the inversion.

A further salient consideration pertains to the disparate slope values derived from the regression lines illustrated in Fig. 9. It is essential to note that, as first-order polynomial linear regressions, these slopes do not accurately represent the true gradients of the identified paleoshorelines. A more precise evaluation would necessitate location-specific assessments or the application of higher-order polynomials that more faithfully capture the dispersion of the sampled data points. This argument is further corroborated by factors relating to the geometry, wavelength, and spatial orientation of the uplift source. As evidenced by the divergent slopes of the FMT and FTN regression lines (Fig. 9), the resultant deformation-induced gradient can exhibit significant variability contingent upon the relative positioning of geomorphological markers versus the uplift source. The precise determination of paleoshoreline slopes presents challenges due to the dispersion of sampled data points and their spatial relationship to the uplift source. Notwithstanding these limitations, we posit that the primary insight derives from the collective set of regression lines, all of which exhibit a negative gradient. This consistent negative slope proves helpful in facilitating the successful inversion of the proposed fault model.

Complementing the tectonic framework of the area, GNSS data provided by Devoti et al. (2017), Fig. 10D) reveal a velocity field in the studied sector that is consistent with a reverse dip-slip motion along the fault (Fig. 3). This information aligns well with our proposed fault model and further substantiates the kinematic behaviour of the tectonic elements in the area. On the other hand, the World Stress Map (Heidbach et al., 2018) data present a more complex picture with two divergent stress directions (Sh_{max}): one observed at Castellammare del Golfo and the other at Palermo (Fig. 3). Castellammare del Golfo's principal stress direction aligns approximately N-S, more compatible with a purely reverse fault motion. In contrast, the principal Sh_{max} direction near Palermo is NW-SE, suggesting a potential for oblique transpressive motion along the fault. While Palermo is closer to the study area, the stress orientation at Castellammare del Golfo aligns more closely with the reverse dip-slip motion indicated by other datasets, adding another layer of complexity to the tectonic setting.

In this sector of the NSCM, the absence of instrumental earthquakes, as recorded in the Catalogo Parametrico dei Terremoti Italiani (CPTI, Rovida et al., 2020), raises questions about the fault's seismic behaviour. The lack of recorded seismic events could suggest longer recurrence intervals or an aseismic nature for the fault. The Database of Individual Seismogenic Sources (DISS Working Group, 2015) lacks information on seismogenic structures for this specific area. Nevertheless, the evidence presented by our study suggests the presence of an active blind fault, emphasizing the need for a reassessment of the potential active geological structures in the area and a more comprehensive characterization of the fault's geometry and kinematics. Such additional data would enable quantitative evaluations of the structure's slip tendency and seismic potential.

6. Conclusive remarks

New insights on the recent tectonic evolution of the Palermo Mountains area have been achieved by a detailed analysis of both geomorphological markers and deposits related to middle-late Quaternary coastline migrations. Paleoshoreline locations, generated by combined glacio-eustatic change and tectonic uplift, have been detected and analyzed by integrating the following methodologies: i) field-coastal survey worked out in the frame of the Geoswim programme and ii) analytic/statistical analysis of high-resolution DEM.

This research documents the relevance, as well as the usefulness, for the reconstruction of the recent tectonic evolution of a coastal area, of the integration of geomorphological surveys of the emerged and submerged coastal belt with the statistical analysis of high-resolution DEM,

and particularly the advantage, but also the limits, of the integration of observations and measures related to both tidal notches and inner edge of marine terraces.

The results not only highlight relevant differences in the elevation of MIS 5.5 littoral deposits and geomorphological markers between +34 and +1.9 m a.s.l., along an N-S transect that depicts an active seaward tilting of the study area but also explain the different elevations of the MIS 5.5 markers in the whole Palermo mountains peninsula. This deformation was generated by the ongoing activity since middle Pleistocene of an ENE-WSW buried fault whose activity has been recorded by the geomorphological markers identified and characterized along the Capo Rama sea cliff (western sector of Palermo Mountains).

Further studies are needed to confirm the actual existence of this buried fault and to assess the implications on the seismotectonic setting of a sector adjacent to the southern Tyrrhenian border, an area characterized by significant seismic activity.

CRediT authorship contribution statement

Mauro Agate: Writing – review & editing, Writing – original draft, Supervision, Resources, Funding acquisition, Formal analysis, Data curation, Conceptualization. **Fabrizio Antonioli:** Writing – review & editing, Writing – original draft, Validation, Supervision, Formal analysis, Data curation, Conceptualization. **Francesco Caldareri:** Writing – review & editing, Writing – original draft, Visualization, Validation, Formal analysis, Data curation, Conceptualization. **Stefano Devoto:** Writing – original draft, Visualization, Data curation, Conceptualization. **Maurizio Gasparo Morticelli:** Writing – review & editing, Writing – original draft, Visualization, Validation, Formal analysis, Data curation, Conceptualization. **Attilio Sulli:** Writing – review & editing, Writing – original draft, Supervision, Resources, Funding acquisition, Data curation, Conceptualization. **Nicolò Parrino:** Writing – review & editing, Writing – original draft, Visualization, Validation, Software, Methodology, Formal analysis, Data curation, Conceptualization. **Stefano Furlani:** Writing – review & editing, Writing – original draft, Supervision, Resources, Methodology, Funding acquisition, Formal analysis, Data curation, Conceptualization.

Declaration of competing interest

The authors declare that they have no known competing financial interests or personal relationships that could have appeared to influence the work reported in this paper.

Acknowledgements

We thank the “Riserva naturale orientata Capo Rama” for the permissions, with mention to Dr. Laura Genco and the “Geoswim programme”, resp. Prof. Stefano Furlani, for the sea research activities.

Data availability

Data will be made available on request.

References

Agate, M., Mancuso, M., Cicero, G., 2005. Late Quaternary sedimentary evolution of the Castellammare Gulf (North-Western Sicily offshore). Boll. Soc. Geol. Ital. 124, 21–40.

Aki, K., Richards, P.G., 2002. Quantitative Seismology. University Science Books, 700 pp.

Albanese, C., Sulli, A., 2012. Backthrusts and passive roof duplexes in fold-and-thrust belts. Tectonophysics 514–517, 180–198. https://doi.org/10.1016/j.tecto.2011.11.002.

Anderson, H., Jackson, J., 1987. Active tectonics of the Adriatic Region. Geophys. J. Int. 91, 937–983. https://doi.org/10.1111/j.1365-246X.1987.tb01675.x.

Antonioli, F., Lo Presti, V., Rovere, A., Ferranti, L., Anzidei, M., Furlani, S., Mastronuzzi, G., Orru, P.E., Scicchitano, G., Sannino, G., Spampinato, C.R., Pagliarulo, R., Deiana, G., De Sabata, E., Sansò, P., Vacchi, M., Vecchio, A., 2015. Tidal notches in Mediterranean Sea: a comprehensive analysis. Quaternary Science Reviews 119, 66–84. https://doi.org/10.1016/j.quascirev.2015.03.016.

Antonioli, F., Anzidei, M., Amorosi, A., Lo Presti, V., Mastronuzzi, G., Deiana, G., De Falco, G., Fontana, A., Fontolan, G., Lisco, S., Marsico, A., Moretti, M., Orrù, P.E., Sannino, G.M., Serpelloni, E., Vecchio, A., 2017. Sea-level rise and potential drowning of the Italian coastal plains: flooding risk scenarios for 2100. Quaternary Science Reviews 158, 29–43. https://doi.org/10.1016/j.quascirev.2016.12.021.

Antonioli, F., Ferranti, L., Stocchi, P., Deiana, G., Lo Presti, V., Furlani, S., Marino, C., Orru, P., Scicchitano, G., Trainito, E., Anzidei, M., Bonamini, M., Sansò, P., Mastronuzzi, G., 2018. Morphometry and elevation of the last interglacial tidal notches in tectonically stable coasts of the Mediterranean Sea. Earth Sci. Rev. 185, 600–623. https://doi.org/10.1016/j.earscirev.2018.06.017.

Antonioli, F., De Falco, G., Lo Presti, V., Moretti, L., Scardino, G., Anzidei, M., Bonaldo, D., Carniel, S., Leoni, G., Furlani, S., Marsico, A., Petitta, M., Randazzo, G., Scicchitano, G., Mastronuzzi, G., 2020. Relative sea-level rise and potential submersion risk for 2100 on 16 coastal plains of the Mediterranean Sea. Water 12, 2173. https://doi.org/10.3390/w12082173.

Antonioli, F., Calcagnile, L., Ferranti, L., Mastronuzzi, G., Monaco, C., Orrù, P., Quarta, G., Pepe, F., Scardino, G., Scicchitano, G., Stocchi, P., Taviani, M., 2021a. New evidence of MIS 3 relative sea level changes from the Messina Strait, Calabria (Italy). Water 13, 2647. https://doi.org/10.3390/w13192647.

Antonioli, F., Furlani, S., Montagna, P., Stocchi, P., 2021b. The use of submerged speleothems for sea level studies in the Mediterranean Sea: a new perspective using Glacial Isostatic Adjustment (GIA). Geosciences 11, 77. https://doi.org/10.3390/geosciences11020077.

Antonioli, F., Furlani, S., Montagna, P., Stocchi, P., Calcagnile, L., Quarta, G., Cecchinel, J., Lo Presti, V., Morticelli, M.G., Foresta Martin, F., Vaccher, V., 2021c. Submerged speleothems and sea level reconstructions: a global overview and new results from the Mediterranean Sea (preprint). Earth Sciences. https://doi.org/10.20944/preprints202105.0100.v1.

Antonioli, F., Agate, A., Ascione, A., Cerrone, P., Deiana, G., Orru, P., Fonta, A., Leoni, G., Monaco, C., Ferranti, L., Mastronuzzi, G., 2023a. Quaternary Map of Italy (Metiq), MIS 5.5 higstand. 5 fogli e note illustrative. In: Italian Geological Survey. ISPRA.

Antonioli, F., Furlani, S., Spada, G., Melini, D., Zomeni, Z., 2023b. The Lambousa (Cyprus) fishtank in a quasi-stable coastal area of the Eastern Mediterranean, a notable marker for testing GIA models. Geosciences 13, 280. https://doi.org/10.3390/geosciences13090280.

Archer, A.W., 2013. World’s highest tides: Hypertidal coastal systems in North America, South America and Europe. Sediment. Geol. 284–285, 1–25. https://doi.org/10.1016/j.sedgeo.2012.12.007.

Bard, E., Hamelin, B., Fairbanks, R.G., 1990. U-Th ages obtained by mass spectrometry in corals from Barbados: sea level during the past 130,000 years. Nature 346, 456–458. https://doi.org/10.1038/346456a0.

Bard, E., Antonioli, F., Silenzi, S., 2002. Sea-level during the penultimate interglacial period based on a submerged stalagmite from Argentarola Cave (Italy). Earth Planet. Sci. Lett. 196 (3–4), 135–146.

Beauducel, F., 2020. Okada: Surface Deformation Due to a Finite Rectangular Source. MATLAB Central File Exchange.

Benac, Č., Juračić, M., Bakran-Petricioli, T., 2004. Submerged tidal notches in the Rijeka Bay NE Adriatic Sea: indicators of relative sea-level change and of recent tectonic movements. Mar. Geol. 212, 21–33. https://doi.org/10.1016/j.margeo.2004.09.002.

Benac, Č., Juračić, M., Blašković, I., 2008. Tidal notches in Vinodol Channel and Bakar Bay, NE Adriatic Sea: indicators of recent tectonics. Mar. Geol. 248, 151–160. https://doi.org/10.1016/j.margeo.2007.10.010.

Billi, A., Presti, D., Faccenna, C., Neri, G., Orecchio, B., 2007. Seismotectonics of the Nubia plate compressive margin in the south Tyrrhenian region, Italy: clues for subduction inception. J. Geophys. Res. 112, 2006JB004837. https://doi.org/10.1029/2006JB004837.

Blanc, A.C., 1936. Una spiaggia pleistocenica a Strombus bu bonius presso Palidoro (Roma). Ist. Ital. di Antropologia.

Blanchon, P., Eisenhauer, A., Fietzke, J., Liebetrau, V., 2009. Rapid sea-level rise and reef back-stepping at the close of the last interglacial highstand. Nature 458, 881–884. https://doi.org/10.1038/nature07933.

Bordoni, P., Valensise, G., 1999. Deformation of the 125 ka marine terrace in Italy: tectonic implications. SP 146, 71–110. https://doi.org/10.1144/GSL.SP.1999.146.01.05.

Caldareri, F., Sulli, A., Parrino, N., Dardanelli, G., Todaro, S., Maltese, A., 2024. On the shoreline monitoring via earth observation: an isoradiometric method. Remote Sens. Environ. 311, 114286.

Cappadonia, C., Di Maggio, C., Agate, M., Agnesi, V., 2020. Geomorphology of the urban area of Palermo (Italy). J. Maps 16 (2), 274–284. https://doi.org/10.1080/17445647.2020.1739154.

Caracausi, A., Sulli, A., 2019. Outgassing of mantle volatiles in compressional tectonic regime away from volcanism: the role of continental delamination. Geochem. Geophys. Geosyst. 20, 2007–2020. https://doi.org/10.1029/2018GC008046.

Castiglioni, G.B., 1979. Geomorfologia. Unione Tipograf.-Ed, Torinese.

Catalano, R., Merlini, S., Sulli, A., 2002. The structure of western Sicily, central Mediterranean. PG 8, 7–18. https://doi.org/10.1144/petgeo.8.1.7.

Catalano, R., Valenti, V., Albanese, C., Accaino, F., Sulli, A., Tinivella, U., Gasparo Morticelli, M., Zanolla, C., Giustiniani, M., 2013a. Sicily’s fold–thrust belt and slab roll-back: the SI.RI.PRO. seismic crustal transect. JGS 170, 451–464. https://doi.org/10.1144/jgs2012-099.

Catalano, R., Basilone, L., Di Maggio, C., Gasparo Morticelli, M., Agate, M., Avellone, G., 2013b. Note illustrative della Carta Geologica d’Italia alla scala 1: 50.000 del Foglio

594–585 “Partinico-Mondello.”. In: Progett CARG Dip di Geol e Geod Univ di Palermo.
Catuneanu, O., Abreu, V., Bhattacharya, J.P., Blum, M.D., Dalrymple, R.W., Eriksson, P. G., Fielding, C.R., Fisher, W.L., Galloway, W.E., Gibling, M.R., Giles, K.A., Holbrook, J.M., Jordan, R., Kendall, C.G.St.C., Macurda, B., Martinsen, O.J., Miall, A.D., Neal, J.E., Nummedal, D., Pomar, L., Posamentier, H.W., Pratt, B.R., Sarg, J.F., Shanley, K.W., Steel, R.J., Strasser, A., Tucker, M.E., Winker, C., 2009. Towards the standardization of sequence stratigraphy. Earth-Science Reviews 92, 1–33. https://doi.org/10.1016/j.earscirev.2008.10.003.
Chappell, J., Omura, A., Esat, T., McCulloch, M., Pandolfi, J., Ota, Y., Pillans, B., 1996. Reconciliaion of late Quaternary sea levels derived from coral terraces at Huon Peninsula with deep sea oxygen isotope records. Earth Planet. Sci. Lett. 141, 227–236. https://doi.org/10.1016/0012-821X(96)00062-3.
Chen, J.H., Curran, H.A., White, B., Wasserburg, G.J., 1991. Precise chronology of the last interglacial 32 period: 234U-230Th data from fossil coral reefs in the Bahamas. Geol. Soc. Am. Bull. 103, 82–97.
Cheney, R.E., 2001. Satellite altimetry. In: Encyclopedia of Ocean Sciences. Elsevier, pp. 58–64. https://doi.org/10.1016/B978-012374473-9.00340-4.
De Gelder, G., Jara-Muñoz, J., Melnick, D., Fernández-Blanco, D., Rouby, H., Pedoja, K., Husson, L., Armijo, R., Lacassin, R., 2020. How do sea-level curves influence modeled marine terrace sequences? Quaternary Science Reviews 229, 106132. https://doi.org/10.1016/j.quascirev.2019.106132.
De Santis, V., Scardino, G., Meschis, M., Ortiz, J.E., Sánchez-Palencia, Y., Caldara, M., 2021. Refining the middle-late Pleistocene chronology of marine terraces and uplift history in a sector of the Apulian foreland (southern Italy) by applying a synchronous correlation technique and amino acid racemization to Patella spp. and Thetystrombus latus. IJG 140, 438–463. https://doi.org/10.3301/IJG.2021.05.
Devoti, R., D’Agostino, N., Serpelloni, E., Pietrantonio, G., Riguzzi, F., Avallone, A., Cavaliere, A., Cheloni, D., Cecere, G., D’Ambrosio, C., Franco, L., Selvaggi, G., Metois, M., Esposito, A., Sepe, V., Galvani, A., Anzidei, M., 2017. A combined velocity field of the Mediterranean Region. Ann. Geophys. 60, 1. https://doi.org/10.4401/ag-7059.
DISS Working Group, 2015. Database of Individual Seismogenic Sources (DISS), version 3.2.0 125 Individual Seismogenic Sources, 167 Composite Seismogenic Sources, 35 Debated Seismogenic Sources. https://doi.org/10.6092/INGV.IT-DISS3.2.0.
Dutton, A., Bard, E., Antonioli, F., Esat, T.M., Lambeck, K., McCulloch, M.T., 2009. Phasing and amplitude of sea-level and climate change during the penultimate interglacial. Nat. Geosci. 2, 355–359. https://doi.org/10.1038/ngeo470.
Emiliani, C., 1955. Pleistocene temperatures. The Journal of Geology 63, 538–578.
Eshagh, M., 2021. Satellite gravimetry observables. In: Satellite Gravimetry and the Solid Earth. Elsevier, pp. 45–90. https://doi.org/10.1016/B978-0-12-816936-0.00002-5.
Fabiani, R., 1941. Tracce di Tirreniano a Strombus bubonius entro la citta` di Palermo. Bollettino Societa` Scienze Naturali ed Economiche XIX, 1–7 (in Italian).
Ferranti, L., Antonioli, F., Mauz, B., Amorosi, A., Dai Pra, G., Mastronuzzi, G., Monaco, C., Orrù, P., Pappalardo, M., Radtke, U., Renda, P., Romano, P., Sansò, P., Verrubbi, V., 2006. Markers of the last interglacial sea-level high stand along the coast of Italy: tectonic implications. Quat. Int. 145–146, 30–54. https://doi.org/10.1016/j.quaint.2005.07.009.
Ferranti, L., Oldow, J., D’Argenio, B., Catalano, R., Lewis, D., Marsella, E., Avellone, G., Maschio, L., Pappone, G., Pepe, F., 2008. Active deformation in Southern Italy, Sicily and southern Sardinia from GPS velocities of the Peri-Tyrrhenian Geodetic Array (PTGA). Bollettino della Società Geologica Italiana 127, 299–316.
Ferranti, L., Santoro, E., Mazzella, M.E., Monaco, C., Morelli, D., 2009. Active transpression in the northern Calabria Apennines, southern Italy. Tectonophysics 476, 226–251. https://doi.org/10.1016/j.tecto.2008.11.010.
Ferranti, L., Burrato, P., Sechi, D., Andreucci, S., Pepe, F., Pascucci, V., 2021. Late Quaternary coastal uplift of southwestern Sicily, central Mediterranean sea. Quaternary Science Reviews 255, 106812. https://doi.org/10.1016/j.quascirev.2021.106812.
Furlani, S., 2020. Integrating observational targets and instrumental data on rock coasts through snorkel surveys: a methodological approach. Mar. Geol. 425, 106191. https://doi.org/10.1016/j.margeo.2020.106191.
Furlani, S., Antonioli, F., 2023. The swim-survey archive of the Mediterranean rocky coasts: potentials and future perspectives. Geomorphology 421, 108529. https://doi.org/10.1016/j.geomorph.2022.108529.
Furlani, S., Cucchi, F., 2013. Downwearing rates of vertical limestone surfaces in the intertidal zone (Gulf of Trieste, Italy). Mar. Geol. 343, 92–98.
Furlani, S., Cucchi, F., Forti, F., Rossi, A., 2009. Comparison between coastal and inland Karst limestone lowering rates in the northeastern Adriatic Region (Italy and Croatia). Geomorphology 104, 73–81.
Furlani, S., Biolchi, S., Cucchi, F., Antonioli, F., Busetti, M., Melis, R., 2011. Tectonic effects on Late Holocene sea level changes in the Gulf of Trieste (NE Adriatic Sea, Italy). Quat. Int. 232, 144–157. https://doi.org/10.1016/j.quaint.2010.06.012.
Furlani, Stefano, Ninfo, A., Zavagno, E., Paganini, P., Zini, L., Biolchi, S., Antonioli, F., Coren, F., Cucchi, F., 2014a. Submerged notches in Istria and the Gulf of Trieste: results from the Geoswim project. Quat. Int. 332, 37–47. https://doi.org/10.1016/j.quaint.2014.01.018.
Furlani, S., Pappalardo, M., Gómez-Pujol, L., Chelli, A., 2014b. Chapter 7 the rock coast of the Mediterranean and Black seas. Memoirs 40, 89–123. https://doi.org/10.1144/M40.7.
Furlani, S., Antonioli, F., Cavallaro, D., Chirco, P., Caldareri, F., Martin, F.F., Morticelli, M.G., Monaco, C., Sulli, A., Quarta, G., Biolchi, S., Sannino, G., de Vita, S., Calcagnile, L., Agate, M., 2017. Tidal notches, coastal landforms and relative sea-level changes during the Late Quaternary at Ustica Island (Tyrrhenian Sea, Italy). Geomorphology 299, 94–106. https://doi.org/10.1016/j.geomorph.2017.10.004.
Furlani, S., Vaccher, V., Antonioli, F., Agate, M., Biolchi, S., Boccali, C., Busetti, A., Caldareri, F., Canziani, F., Chemello, R., Deguara, J.C., Bo, E.D., Dean, S., Deiana, G., De Sabata, E., Donno, Y., Gauci, R., Giaccone, T., Lo Presti, V., Montagna, P., Navone, A., Orrù, P.E., Porqueddu, A., Schembri, J.A., Taviani, M., Torricella, F., Trainito, E., Vacchi, M., Venturini, E., 2021. Preservation of modern and mis 5.5 erosional landforms and biological structures as sea level markers: a matter of luck? Water (Switzerland) 13. https://doi.org/10.3390/w13152127.
Gasparo Morticelli, M., Valenti, V., Catalano, R., Sulli, A., Agate, M., Avellone, G., Albanese, C., Basilone, L., Gugliotta, C., 2015. Deep controls on foreland basin system evolution along the Sicilian fold and thrust belt. Bulletin de la Société Géologique de France 186, 273–290. https://doi.org/10.2113/gssgfbull.186.4-5.273.
Gignoux, M., 1913. Les formations marines pliocenes et quaternaires de l’Italie du Sud et de la Sicilie. Ann. Univ. Lyon 35, 1–693.
Goes, S., Giardini, D., Jenny, S., Hollenstein, C., Kahle, H.-G., Geiger, A., 2004. A recent tectonic reorganization in the south-central Mediterranean. Earth Planet. Sci. Lett. 226, 335–345. https://doi.org/10.1016/j.epsl.2004.07.038.
Hearty, P.J., 1986. An inventory of last Interglacial (sensu lato) age deposits from the Mediterranean basin: a study of isoleucine epimerization and U-series dating. Z. Geomorphol. 62, 51–69.
Hearty, P.J., Dai Pra, G., 1987. Ricostruzione paleogeografica degli ambienti litoranei quaternari della Toscana e del Lazio settentrionale con l’impiego dell’aminostratigrafia. Boll. Servizio Geologico d’Italia 106, 189–224.
Heidbach, O., Rajabi, M., Cui, X., Fuchs, K., Müller, B., Reinecker, J., Reiter, K., Tingay, M., Wenzel, F., Xie, F., Ziegler, M.O., Zoback, M.-L., Zoback, M., 2018. The World Stress Map database release 2016: crustal stress pattern across scales. Tectonophysics 744, 484–498. https://doi.org/10.1016/j.tecto.2018.07.007.
Huggett, R., Shuttleworth, E., 2022. Fundamentals of Geomorphology. Taylor & Francis.
Jara-Muñoz, J., Melnick, D., Pedoja, K., Strecker, M.R., 2019. TerraceM-2: a Matlab® interface for mapping and modeling marine and lacustrine terraces. Front. Earth Sci. 7, 255. https://doi.org/10.3389/feart.2019.00255.
Komori, J., Ando, R., Shishikura, M., 2020. Cluster analysis of marine terraces and quantitative seismotectonic interpretation of the Boso Peninsula, Central Japan. JGR Solid Earth 125, e2019JB019211. https://doi.org/10.1029/2019JB019211.
Komori, J., Shishikura, M., Ando, R., Yokoyama, Y., Miyairi, Y., 2021. A Bayesian approach to age estimation of marine terraces and implications for the history of the great Kanto earthquakes, central Japan. Quaternary Science Reviews 272, 107217. https://doi.org/10.1016/j.quascirev.2021.107217.
Kopp, R.E., Simons, F.J., Mitrovica, J.X., Maloof, A.C., Oppenheimer, M., 2009. Probabilistic assessment of sea level during the last interglacial stage. Nature 462, 863–867. https://doi.org/10.1038/nature08686.
Lambeck, K., Bard, E., 2000. Sea-level change along the French Mediterranean coast for the past 30 000 years. Earth Planet. Sci. Lett. 175, 203–222. https://doi.org/10.1016/S0012-821X(99)00289-7.
Lambeck, K., Antonioli, F., Purcell, A., Silenzi, S., 2004. Sea-level change along the Italian coast for the past 10,000yr. Quaternary Science Reviews 23, 1567–1598. https://doi.org/10.1016/j.quascirev.2004.02.009.
Lambeck, K., Antonioli, F., Anzidei, M., Ferranti, L., Leoni, G., Scicchitano, G., Silenzi, S., 2011. Sea level change along the Italian coast during the Holocene and projections for the future. Quat. Int. 232, 250–257. https://doi.org/10.1016/j.quaint.2010.04.026.
Lo Presti, V., Antonioli, F., Auriemma, R., Ronchitelli, A., Scicchitano, G., Spampinato, C. R., Anzidei, M., Agizza, S., Benini, A., Ferranti, L., 2014. Millstone coastal quarries of the Mediterranean: a new class of sea level indicator. Quat. Int. 332, 126–142. https://doi.org/10.1016/j.quaint.2014.03.021.
Lorscheid, T., Felis, T., Stocchi, P., Obert, J.C., Scholz, D., Rovere, A., 2017. Tides in the Last Interglacial: insights from notch geometry and palaeo tidal models in Bonaire, Netherland Antilles. Sci Rep 7, 16241. https://doi.org/10.1038/s41598-017-16285-6.
Maiorana, M., Parente, F., Sulli, A., Todaro, S., Caldareri, F., Agate, M., 2024. Fluid seepage evidence in the Adventure Plateau (NW Sicily Channel).
Malatesta, A., 1985. Geologia e paleobiologia dell’era glaciale. In: La Nuova Italia Scientifica, 282 pp.
Malatesta, L.C., Finnegan, N.J., Huppert, K.L., Carreño, E.I., 2022. The influence of rock uplift rate on the formation and preservation of individual marine terraces during multiple sea-level stands. Geology 50, 101–105. https://doi.org/10.1130/G49245.1.
Malik, J.N., Srivastava, E., Gadhavi, M.S., Livio, F., Sharma, N., Arora, S., Sulli, A., 2024. Holocene surface-rupturing paleo-earthquakes along the Kachchh Mainland Fault: shaping the seismic landscape of Kachchh, Western India. Scientific Reports 14 (1), 11612.
Maltese, A., Caldareri, F., Dardanelli, G., Todaro, S., Parrino, N., Sulli, A., 2024. On the shoreline positioning via remote sensing imagery: an isoradiometric approach. J. Appl. Remote. Sens. 18 (1), 014529.
Mariucci, M.T., Montone, P., 2020. Database of Italian present-day stress indicators, IPSI 1.4. Sci Data 7, 298. https://doi.org/10.1038/s41597-020-00640-w.
Mastrolembo Ventura, B., Serpelloni, E., Argnani, A., Bonforte, A., Bürgmann, R., Anzidei, M., Baldi, P., Puglisi, G., 2014. Fast geodetic strain-rates in eastern Sicily (southern Italy): new insights into block tectonics and seismic potential in the area of the great 1693 earthquake. Earth Planet. Sci. Lett. 404, 77–88. https://doi.org/10.1016/j.epsl.2014.07.025.
Mauz, B., Buccheri, G., Zöller, L., Greco, A., 1997. Middle to Upper Pleistocene morphostructural evolution of the NW-coast of Sicily: thermoluminescence dating and palaeontological-stratigraphical evaluations of littoral deposits. Palaeogeogr. Palaeoclimatol. Palaeoecol. 128, 269–285. https://doi.org/10.1016/s0031-0182(96)00033-8.

Mauz, B., Sivan, D., Galili, E., 2020. MIS 5e sea-level proxies in the eastern Mediterranean coastal region (preprint). Geosciences – Mar. Geol. https://doi.org/10.5194/essd-2020-357.
Meschis, M., Romano, D., Palano, M., Scicchitano, G., De Santis, V., Scardino, G., Gattuso, A., Caruso, C.G., Sposito, F., Lazzaro, G., Sciré Scappuzzo, S.S., Semprebello, A., Morici, S., Longo, M., 2024. Crustal uplift rates implied by synchronously investigating Late Quaternary marine terraces in the Milazzo Peninsula, Northeast Sicily, Italy. In: Earth Surface Processes and Landforms.
Milia, A., Iannace, P., Tesauro, M., Torrente, M.M., 2018. Marsili and Cefalù basins: the evolution of a rift system in the southern Tyrrhenian Sea (Central Mediterranean). Global Planet. Change 171, 225–237. https://doi.org/10.1016/j.gloplacha.2017.12.003.
Mosegaard, K., Tarantola, A., 1995. Monte Carlo sampling of solutions to inverse problems. J. Geophys. Res. Solid Earth 100, 12431–12447. https://doi.org/10.1029/94JB03097.
Muhs, D.R., Simmons, K.R., 2017. Taphonomic problems in reconstructing sea-level history from the late Quaternary marine terraces of Barbados. Quatern. Res. 88, 409–429. https://doi.org/10.1017/qua.2017.70.
Murray-Wallace, C.V., Woodroffe, C.D., 2014. Quaternary Sea-Level Changes: A Global Perspective, 1st ed. Cambridge University Press. https://doi.org/10.1017/CBO9781139024440.
Nisi, M.F., Antonioli, F., Pra, G.D., Leoni, G., Silenzi, S., 2003. Coastal deformation between the Versilia and the Garigliano plains (Italy) since the last interglacial stage. J Quaternary Science 18, 709–721. https://doi.org/10.1002/jqs.803.
Okada, Y., 1985. Surface deformation due to shear and tensile faults in a half-space. Bull. Seismol. Soc. Am. 75, 1135–1154. https://doi.org/10.1785/BSSA0750041135.
Parrino, N., Agosta, F., Di Stefano, P., Napoli, G., Pepe, F., Renda, P., 2019. Fluid storage and migration properties of sheared Neptunian dykes. Mar. Pet. Geol. 102, 521–534. https://doi.org/10.1016/j.marpetgeo.2019.01.008.
Parrino, N., Pepe, F., Burrato, P., Dardanelli, G., Corradino, M., Pipitone, C., Morticelli, M.G., Sulli, A., Di Maggio, C., 2022. Elusive active faults in a low strain rate region (Sicily, Italy): hints from a multidisciplinary land-to-sea approach. Tectonophysics 839, 229520. https://doi.org/10.1016/j.tecto.2022.229520.
Parrino, N., Burrato, P., Sulli, A., Gasparo Morticelli, M., Agate, M., Srivastava, E., Malik, J.N., Di Maggio, C., 2023. Plio-Quaternary coastal landscape evolution of north-western Sicily (Italy). J. Maps 1–13. https://doi.org/10.1080/17445647.2022.2159889.
Pedoja, K., Husson, L., Regard, V., Cobbold, P.R., Ostanciaux, E., Johnson, M.E., Kershaw, S., Saillard, M., Martinod, J., Furgerot, L., Weill, P., Delcaillau, B., 2011. Relative sea-level fall since the last interglacial stage: are coasts uplifting worldwide? Earth-Science Reviews 108, 1–15. https://doi.org/10.1016/j.earscirev.2011.05.002.
Peltier, W.R., 2004. Global Glacial isostasy and the surface of the ice-age earth: the ICE-5G (VM2) model and grace. Annu. Rev. Earth Planet. Sci. 32, 111–149. https://doi.org/10.1146/annurev.earth.32.082503.144359.
Pirazzoli, P.A., Evelpidou, N., 2013. Tidal notches: a sea-level indicator of uncertain archival trustworthiness. Palaeogeogr. Palaeoclimatol. Palaeoecol. 369, 377–384. https://doi.org/10.1016/j.palaeo.2012.11.004.
Pirrotta, C., Parrino, N., Pepe, F., Tansi, C., Monaco, C., 2022. Geomorphological and morphometric analyses of the catanzaro trough (Central Calabrian Arc, Southern Italy): seismotectonic implications. Geosciences 12, 324. https://doi.org/10.3390/geosciences12090324.
Pondrelli, S., Visini, F., Rovida, A., D'Amico, V., Pace, B., Meletti, C., 2020. Style of faulting of expected earthquakes in Italy as an input for seismic hazard modeling. Nat. Hazards Earth Syst. Sci. 20, 3577–3592. https://doi.org/10.5194/nhess-20-3577-2020.
Racano, S., Jara-Muñoz, J., Cosentino, D., Melnick, D., 2020. Variable quaternary uplift along the southern margin of the Central Anatolian Plateau inferred from modeling marine terrace sequences. Tectonics 39, e2019TC005921. https://doi.org/10.1029/2019TC005921.
Ramos, N.T., Tsutsumi, H., 2010. Evidence of large prehistoric offshore earthquakes deduced from uplifted Holocene marine terraces in Pangasinan Province, Luzon Island, Philippines. Tectonophysics 495, 145–158. https://doi.org/10.1016/j.tecto.2010.08.007.
Ramos, N.T., Tsutsumi, H., Perez, J.S., Bermas, P.P., 2012. Uplifted marine terraces in Davao Oriental Province, Mindanao Island, Philippines and their implications for large prehistoric offshore earthquakes along the Philippine trench. J. Asian Earth Sci. 45, 114–125. https://doi.org/10.1016/j.jseaes.2011.07.028.
Regione Siciliana, 2010. Modello digitale del terreno (MDT) 2m x 2m Regione Siciliana-ATA 2007-2008 [WWW Document]. URL. http://www.sitr.regione.sicilia.it.
Roberts, G.P., Meschis, M., Houghton, S., Underwood, C., Briant, R.M., 2013. The implications of revised Quaternary palaeoshoreline chronologies for the rates of active extension and uplift in the upper plate of subduction zones. Quat. Sci. Rev. 78, 169–187. https://doi.org/10.1016/j.quascirev.2013.08.006.
Robertson, J., Roberts, G.P., Iezzi, F., Meschis, M., Gheorghiu, D.M., Sahy, D., Bristow, C., Sgambato, C., 2020. Distributed normal faulting in the tip zone of the South Alkyonides Fault System, Gulf of Corinth, constrained using 36Cl exposure dating of late-Quaternary wave-cut platforms. J. Struct. Geol. 136, 104063. https://doi.org/10.1016/j.jsg.2020.104063.
Rosendahl Appelquist, L., 2012. Generic framework for meso-scale assessment of climate change hazards in coastal environments. J. Coast. Conserv. 17. https://doi.org/10.1007/s11852-012-0218-z.
Rovere, A., Ryan, D.D., Vacchi, M., Dutton, A., Simms, A.R., Murray-Wallace, C.V., 2023. The World Atlas of Last Interglacial Shorelines (version 1.0). Earth Syst. Sci. Data 15, 1–23. https://doi.org/10.5194/essd-15-1-2023.
Rovida, A., Locati, M., Romano, C., Lolli, B., Gasperini, P., 2020. The Italian earthquake catalogue CPTI15. Bull. Earthq. Eng. 18. https://doi.org/10.1007/s10518-020-00818-y.
Ruggieri, G., Unti, M., 1974. Pliocene e Pleistocene nell'entroterra di Marsala. Estratto dal Bollettino Società Geologica Italiana 93, 723–733, 3 ff., Roma.
Santoro, E., Ferranti, L., Burrato, P., Mazzella, M.E., Monaco, C., 2013. Deformed Pleistocene marine terraces along the Ionian Sea margin of southern Italy: unveiling blind fault-related folds contribution to coastal uplift. Tectonics 32, 737–762. https://doi.org/10.1002/tect.20036.
Schellmann, G., Radtke, U., 2004. A revised morpho- and chronostratigraphy of the Late and Middle Pleistocene coral reef terraces on Southern Barbados (West Indies). Earth-Science Reviews 64, 157–187. https://doi.org/10.1016/S0012-8252(03)00043-6.
Schwanghart, W., Scherler, D., 2014. TopoToolbox 2–MATLAB-based software for topographic analysis and modeling in Earth surface sciences. Earth Surf. Dyn. 2, 1–7.
Shackleton, N.J., Opdyke, N.D., 1973. Oxygen isotope and palaeomagnetic stratigraphy of Equatorial Pacific core V28-238: oxygen isotope temperatures and ice volumes on a 105 year and 106 year scale. Quatern. Res. 3, 39–55.
Shackleton, N.J., Sánchez-Goñi, M.F., Pailler, D., Lancelot, Y., 2003. Marine isotope substage 5e and the Eemian interglacial. Global Planet. Change 36, 151–155. https://doi.org/10.1016/S0921-8181(02)00181-9.
Srivastava, E., Malik, J.N., Parrino, N., Burrato, P., Sharma, N., Gadhavi, M., Sulli, A., Di Maggio, C., Morticelli, M.G., 2023. Extremely fast Holocene coastal landscape evolution in the Kachchh Upland (NW India): clues from a multidisciplinary review. J. Maps 1–10. https://doi.org/10.1080/17445647.2023.2167617.
Stirling, C.H., Esat, T.M., Lambeck, K., McCulloch, M.T., 1998. Timing and duration of the Last Interglacial: evidence for a restricted interval of widespread coral reef growth. Earth Planet. Sci. Lett. 160, 745–762. https://doi.org/10.1016/S0012-821X(98)00125-3.
Sulli, A., Morticelli, M.G., Agate, M., Zizzo, E., 2019. Hinterland-verging thrusting in the Northern Sicily continental margin: evidences for a late collisional stage of the Sicilian fold and thrust belt? In: Rossetti, F., Blanc, A.C., Riguzzi, F., Leroux, E., Pavlopoulos, K., Bellier, O., Kapsimalis, V. (Eds.), The Structural Geology Contribution to the Africa-Eurasia Geology: Basement and Reservoir Structure, Ore Mineralisation and Tectonic Modelling, Advances in Science, Technology & Innovation. Springer International Publishing, Cham, pp. 251–253. https://doi.org/10.1007/978-3-030-01455-1_54.
Sulli, A., Gasparo Morticelli, M., Agate, M., Zizzo, E., 2021a. Active north-vergent thrusting in the northern Sicily continental margin in the frame of the quaternary evolution of the Sicilian collisional system. Tectonophysics 802, 228717. https://doi.org/10.1016/j.tecto.2021.228717.
Sulli, A., Zizzo, E., Spatola, D., Morticelli, M.G., Agate, M., Iacono, C.L., Gargano, F., Pepe, F., Ciaccio, G., 2021b. Growth and geomorphic evolution of the Ustica volcanic complex at the Africa-Europe plate margin (Tyrrhenian Sea). Geomorphology 374, 107526. https://doi.org/10.1016/j.geomorph.2020.107526.
Sunamura, T., 1992. Geomorphology of Rocky Coasts. Wiley.
Todaro, S., Agosta, F., Parrino, N., Cavalcante, F., Di Stefano, P., Giarrusso, R., Pepe, F., Renda, P., Tondi, E., 2022. Fracture stratigraphy and oil first migration in Triassic shales, Favignana Island, western Sicily, Italy. Marine and Petroleum Geology 135, 105400. https://doi.org/10.1016/j.marpetgeo.2021.105400.
Vacchi, M., Rovere, A., Zouros, N., Desruelles, S., Caron, V., Firpo, M., 2012. Spatial distribution of sea-level markers on Lesvos Island (NE Aegean Sea): evidence of differential relative sea-level changes and the neotectonic implications. Geomorphology 159–160, 50–62. https://doi.org/10.1016/j.geomorph.2012.03.004.
Vail, P.R., Mitchum Jr, R.M., Thompson III, S., 1977. Seismic stratigraphy and global changes of sea level: Part 3. Relative changes of sea level from Coastal Onlap: section 2. In: Application of seismic reflection Configuration to Stratigrapic Interpretation.
Vail, P.R., Hardenbol, J., Todd, R.G., 1984. Jurassic unconformities, chronostratigraphy and sea-level changes from seismic stratigraphy and biostratigraphy.
Zazo, C., Silva, P.G., Goy, J.L., Hillaire-Marcel, C., Ghaleb, B., Lario, J., Bardají, T., González, A., 1999. Coastal uplift in continental collision plate boundaries: data from the Last Interglacial marine terraces of the Gibraltar Strait area (south Spain). Tectonophysics 301, 95–109. https://doi.org/10.1016/S0040-1951(98)00217-0.
Zitellini, N., Ranero, C.R., Loreto, M.F., Ligi, M., Pastore, M., D'Oriano, F., Sallares, V., Grevemeyer, I., Moeller, S., Prada, M., 2020. Recent inversion of the Tyrrhenian Basin. Geology 48, 123–127. https://doi.org/10.1130/G46774.1.